Lewis Pairing and Frustration of Group 13/15 Elements Geometrically Enforced by (Ace)Naphthalene, Biphenylene and (Thio)Xanthene Backbones

Omar Sadek, Ghenwa Bouhadir, Didier Bourissou

Lewis Pairing and Frustration of Group 13/15 Elements Geometrically Enforced by (Ace)Naphthalene, Biphenylene and (Thio)Xanthene Backbones

Omar Sadek,[a]* Ghenwa Bouhadir[a] and Didier Bourissou[a]*

[a]CNRS/Université Toulouse III - Paul Sabatier, Laboratoire Hétérochimie Fondamentale et Appliquée (LHFA, UMR 5069)

118 Route de Narbonne, 31062 Toulouse Cedex 09 (France)

E-mail: dbouriss@chimie.ups-tlse.fr

Homepage: http://lhfa.cnrs.fr/index.php/equipes/lbpb/accueil-lbpb

Abstract:

The synthesis, structure, and reactivity of mixed group 13/group 15 compounds (E^{13} = B, Al, Ga, In; E^{15} = N, P, Sb, Bi) featuring a rigid (ace)naphthalene or (thio)xanthene backbone are discussed in this review. The backbone may either enforce or prevent $E^{15} \rightarrow E^{13}$ interactions, resulting in Lewis pairing or frustration. The formation of strong $E^{15} \rightarrow E^{13}$ interactions is possible upon peri-substitution of (ace)naphthalenes. This gives the opportunity to access and study highly reactive species, as exemplified by P-stabilised borenium salts and boryl radicals. In turn, rigid expanded spacers such as biphenylenes, (thio)xanthenes and dibenzofurans impose long distances and geometrically prevent $E^{15} \rightarrow E^{13}$ interactions. Such P-B derivatives display ambiphilic coordination properties and frustrated Lewis pair behaviour towards small molecules, their preorganised structure favouring reversible interaction/activation. Throughout the review, the importance of the scaffold in enforcing or preventing $E^{15} \rightarrow E^{13}$ interactions is highlighted and discussed based on experimental data and theoretical calculations.

Introduction

Donor-acceptor (D→A) interactions is a field of huge interest and intense research. They are present in a broad range of chemical structures that find applications in many fields including organic synthesis, catalysis and materials science.

Connecting donor and acceptor moieties through an organic linker is very appealing. This provides a degree of control over the D→A interaction by tuning the length and rigidity of the spacer. In this context, rigid carbon-based scaffolds have attracted much interest over the last two decades. This review summarizes the advances made on mixed group 13/group 15 compounds (E^{13} = B, Al, Ga, In; E^{15} = N, P, Sb, Bi) in which the D and A sites are maintained in proximity (as with naphthalene or acenaphthalene) or far from each other (as with biphenylene, xanthene, thioxanthene or dibenzofuran) (Chart 1).

Emphasis is given to the synthetic access to these derivatives, as well as their electronic and structural features. Their reactivity is also discussed, particularly in the context of small molecule activation and generation of highly reactive B species thanks to geometrically enforced, stabilising P→B interactions.

Throughout the review, the ability of the rigid backbone to enforce or prevent intramolecular E^{15}→E^{13} interaction is discussed and analysed based on spectroscopic, structural and theoretical considerations. In general, *peri*-substitution of (ace)naphthalenes tends to enforce E^{15}→E^{13} interaction (Lewis pairing), but the juxtaposition of the E^{15}- and E^{13}-based groups induces strong constraints. In contrast, xanthene, thioxanthene and dibenzofuran prevent E^{15}→E^{13} interaction (Lewis pair frustration) due to the imposed distance between the D and A sites. Of note, the (ace)naphthalene, xanthene and dibenzofuran scaffolds are essentially planar, whereas the large size of S and the presence of a sp^3-hybridized carbon atom in the central ring make thioxanthenes to fold. The geometric difference between the various spacers is clearly apparent from the corresponding H···H distance in the respective frameworks, from ~2.45 and 2.67 Å in naphthalene[1] and acenaphthalene,[2] to 3.82, 4.55, 5.11 and 5.22 Å in biphenylene,[3] xanthene,[4] thioxanthene[5] and difenzofuran,[6] respectively (Chart 1).

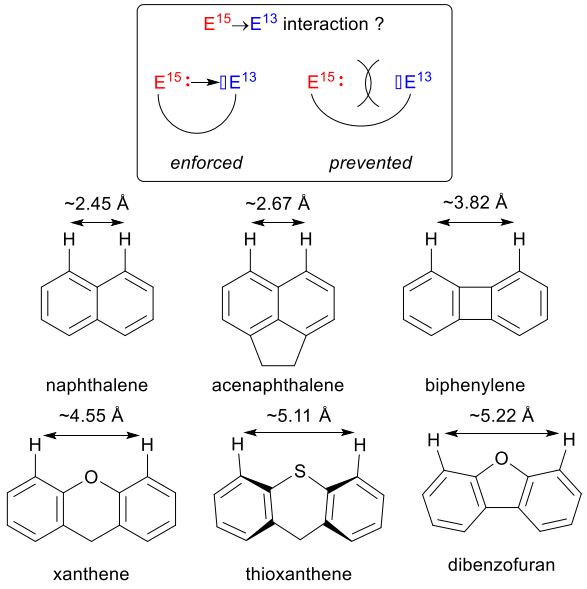

Chart 1 Schematic representation of the mixed group 13/group 15 compounds covered in this review in their two limit forms (with/without E^{15}→E^{13} interaction); corresponding carbon-based spacers with the nominal distance between the *peri* (and *peri*-like) positions.

2. Generalities

Synthesis of (ace)naphthalenes, (thio)xanthenes and dibenzofurans featuring group 13/15 elements. For brevity and to avoid repetition, the synthetic pathways used to access these derivatives are presented below.

Directed lithiation and halogen-lithium exchange reactions followed by electrophilic trapping. Most compounds discussed in this review were prepared by ionic coupling, as illustrated schematically in Scheme 1 for (ace)naphthalene derivatives. Functionalisation of the (ace)naphthyl framework usually begins by the incorporation of the group 15 moiety followed by the group 13 atom, although in certain cases, the order can be reversed (*vide infra*). The key step is the electrophilic trapping of a E^{15}-functionalized organometallic intermediate, typically an organolithium derivative, with an appropriate E^{13}-based electrophile. The organolithium species is generated either by direct lithiation (N-directed metalation) or halogen-lithium exchange. Occasionally, the E^{13}-based electrophile is reacted after lithium-tin exchange. The same methodology was used to obtain the related biphenylene, (thio)xanthene and dibenzofuran compounds, in which the two positions to functionalize with E^{15}/E^{13} elements are far from each other.

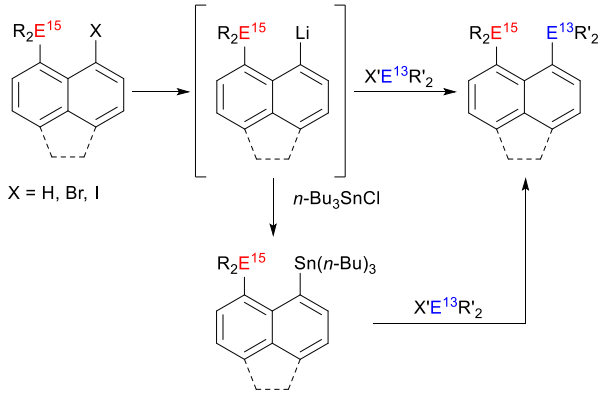

Scheme 1 Schematic representation of the general synthetic route used to access E^{15}/E^{13} *peri* substituted (ace)naphthyl derivatives and related compounds.

Two other synthetic routes have been developed in the case of N-B derivatives. They are far less general but are briefly discussed hereafter for sake of comprehensiveness.

Transition-metal-catalysed borylation reactions. Among the numerous transition-metal-catalysed borylation reactions described in the literature,[7,8] one example deals with a naphthalene compound *peri*-substituted with dimethylamino and pinacolborane moieties (Scheme 2, top).[9] It is obtained in high yield by C–Br activation and C–B coupling from the respective naphthyl amine. Also noteworthy is the possibility to achieve direct C–H borylation. This approach has been applied to benzo*[h]*quinoline (affording naphthalene-like N(sp^2)-B compounds) using Pd, Ru or Rh catalysts (Scheme 2, bottom).[10–15] This borylation is efficient in the case of pinacol- and catecholboranes, but only poor yield was achieved with 9-borabicyclo[3.3.1]nonane (9-BBN).

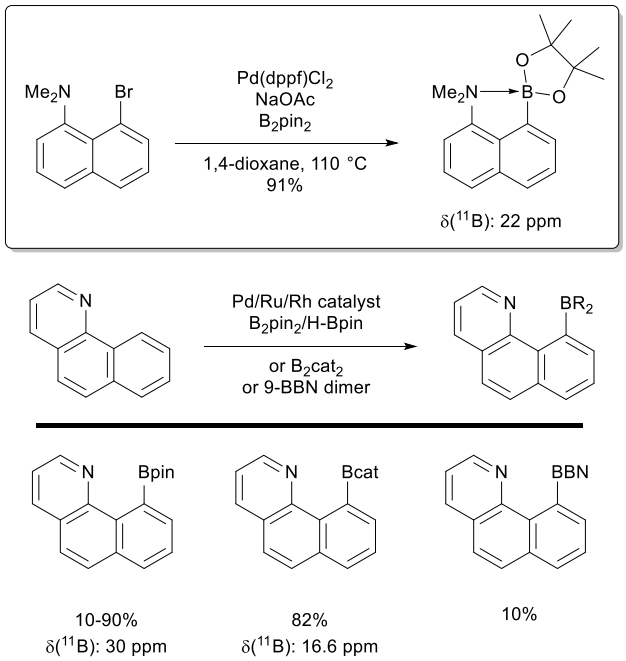

Scheme 2 Transition-metal-catalysed borylations of naphthalene (top) and benzo[*h*]quinoline (bottom) scaffolds.

Diels-Alder reactions with borylbenzynes. Akai *et al.* reported in 2010 a two-step synthesis of a functionalized naphthyl-bridged amine-borane. It starts by Diels-Alder (DA) reaction of borylbenzynes with pyrroles (Scheme 3).[16] Using borylated *o*-iodophenyl triflates as benzyne precursors, the DA adducts were prepared in good to excellent yields and high regioselectivity. According to DFT calculations, the regioselectivity of these DA reactions is controlled by electrostatic effects and the aryne distortion induced by the boryl group.[17] Acid-catalysed isomerization with *p*-TsOH then proceeds easily and quantitatively to give the corresponding N-B naphthyl compound.

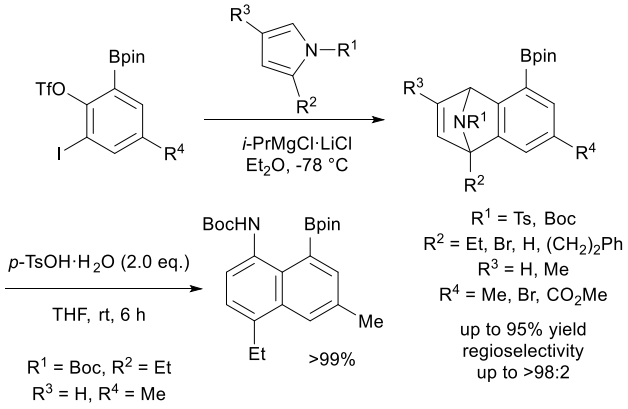

Scheme 3 Synthesis of a naphthyl-bridged amine-borane by Diels-Alder reaction of borylbenzynes with substituted pyrroles, followed by acid-catalysed isomerization.

Probing the presence and strength of $E^{15}\rightarrow E^{13}$ interactions.

Spectroscopic parameters. NMR spectroscopy is a very powerful tool in the assessment of the electronic state of both *peri* substituents, providing valuable insight into their D→A relationship and allowing for (preliminary) evaluation of the structural and bonding situation as well as potential reactivity. Whenever possible, relevant NMR data will be summarized, compared and discussed. Notably, in the case of boron, ^{11}B NMR is highly sensitive and diagnostic with respect to the degree

of coordination about the B centre. Tricoordinate B centres typically display NMR signals in the range of 80-30 ppm while tetracoordinate B centres display signals from 20 to -20 ppm, depending on the substituents on B. Similarly, the signal observed by ^{31}P NMR is highly indicative of the P environment. It is a good probe for the interaction of the P lone pair (lp) with the acceptor moiety. Note that typical coupling descriptors have been used to describe the NMR signals (s, singlet; d, doublet; t, triplet; q, quartet; pseudo q: 1:1:1:1 P-B coupling; br: broad).

Structural parameters. Two limit forms can be envisioned for *peri*-substituted (ace)naphthalenes: one open form, free of a $E^{15}\rightarrow E^{13}$ interaction, and one closed form, with a $E^{15}\rightarrow E^{13}$ interaction. When suitable crystals can be obtained, X-ray diffraction analysis is the most diagnostic way to assess the structure adopted by a given compound, although in some cases crystal packing may come into play and the solid-state structure may not be representative of the ground state. Whenever available, the relevant structural parameters (Chart 2) will be highlighted and compared to assess the bonding situation, particularly with respect to the possible $E^{15}\rightarrow E^{13}$ interaction. The distance between the two elements (E^{15}-E^{13}) is a pivotal indicator. In addition, the ratio between the E^{15}-E^{13} distance and the sum of the covalent radii of the respective elements, referred to as *r*, is most useful when comparing the strength of D→A interactions across different elements. The stronger the $E^{15}\rightarrow E^{13}$ interaction is, the closer the *r* value to 1 is.

The propensity of the (ace)naphthene framework to enforce or prevent the formation of $E^{15}\rightarrow E^{13}$ donor-acceptor interactions can also be assessed by the geometry of the E^{13} centre. When possible, the sum of angles about E^{13} ($\Sigma_\alpha E^{13}$) will be reported as an evaluation of the pyramidalization of the E^{13} centre. A trigonal planar centre free of $E^{15}\rightarrow E^{13}$ interaction has $\Sigma_\alpha E^{13} = 360°$ and the sum of angles $\Sigma_\alpha E^{13}$ decreases as the $E^{15}\rightarrow E^{13}$ interaction strengthens. When dealing with four-coordinate E^{13} elements, the tetrahedral character (THC), as introduced by Höpfl *et al.* to evaluate N→B interactions,[18] is a valuable complementary descriptor. Whenever relevant, it is reported and correlated to the $E^{15}\rightarrow E^{13}$ bond length, to assess the strength of the $E^{15}\rightarrow E^{13}$ interaction.

The bay angles, E^{15}-C_{peri}-C_{bridge}, C_{peri}-C_{bridge}-C_{peri} and C_{bridge}-C_{peri}-E^{13}, and their deviation from the ideal 120° value provides an idea of the extent of in-plane distortion of the (ace)naphthalene scaffolds. On the other hand, out-of-plane distortion can be evaluated using torsion angles, most commonly $\varphi = E^{15}$-$C_{peri}\cdots C_{peri}$-E^{13}, as well as the deviations of the *peri* groups from the mean (ace)naphthalene plane (α/α' or d/d', recall Chart 2). The (ace)naphthalene scaffold itself can distort to respond to and accommodate significant steric crowding imposed by both *peri* substituents. This is generally assessed by torsion angles of the two six-membered rings around the central C–C bond.

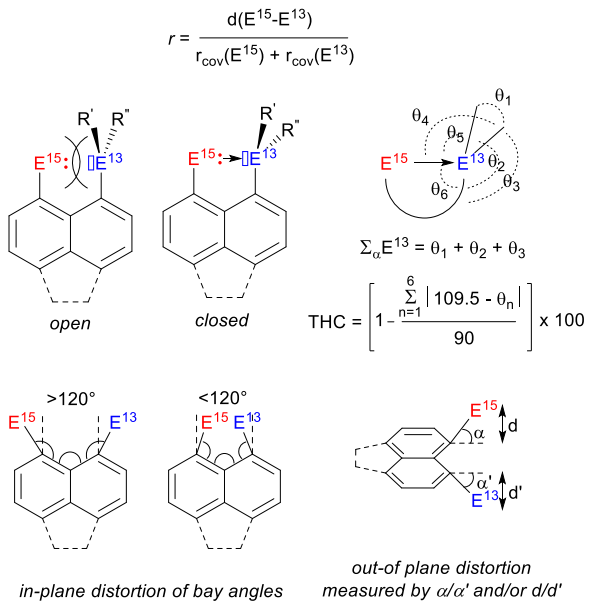

Chart 2 Schematic representation of the most relevant structural parameters used to describe the E^{15}→E^{13} interaction and the (ace)naphthalene distortion.

Peri-Interaction Energy. To assess the stabilisation/destabilisation induced by the presence of E^{15}/E^{13} *peri* substituents in (ace)naphthalene scaffolds, Mebs, Beckmann *et al.* refer to the *peri*-interaction energy (α-PIE).[19] This calculation involves an isodesmic reaction between the disubstituted compound E^{15}-E^{13}, the unsubstituted compound HH and the two monosubstituted compounds E^{15}H and E^{13}H (Scheme 4). This parameter accounts for the stabilization achieved through the D→A interaction between E^{15} and E^{13} while also considering the loss in energy via the steric repulsion encountered by the *peri* substituents and the distortion induced by the presence of E^{15} and E^{13} in such close proximity. In effect, the α-PIE is a measure of the gain or loss in energy upon the juxtaposition of E^{15} and E^{13}. Negative α-PIE energies are indicative of regular Lewis pairs with attractive *peri* interactions, while repulsive *peri* interactions result in positive α-PIE values, classifying these derivatives as frustrated Lewis pairs (FLPs). As highlighted by Mebs and Beckmann, in certain cases, regular Lewis pairs may display positive α-PIE values. This is when *peri* interactions are predominantly repulsive despite the presence of a E^{15}→E^{13} interaction.

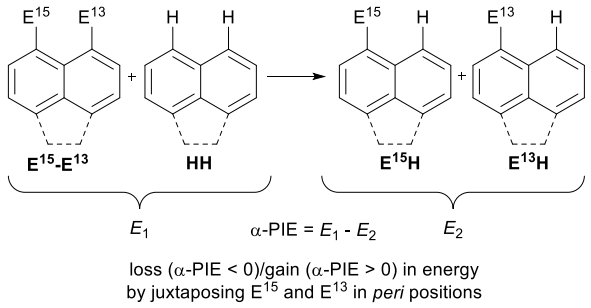

Scheme 4 Isodesmic reaction for the calculation of α-PIE.

3.1. (Ace)naphthalene N-B derivatives

One of the first E^{15}-E^{13} *peri*-substituted naphthalene compound described was the amine-borane **1**, synthesised in 1988 in low yield by quenching 8-lithio-*N,N*-dimethyl-1-naphthylamine with $BF_3{\cdot}OEt_2$ in the presence of excess *n*-BuLi (Scheme 5).[20] While not characterised in the solid-state, ^{11}B NMR spectroscopy points to the presence of a tetracoordinate B centre with an upfield signal at 9.1 ppm.

The strength of the N→B interaction was evidenced by the resistance of this derivative to oxidation even under harsh conditions (refluxing with 3 M NaOH and 30% H_2O_2).

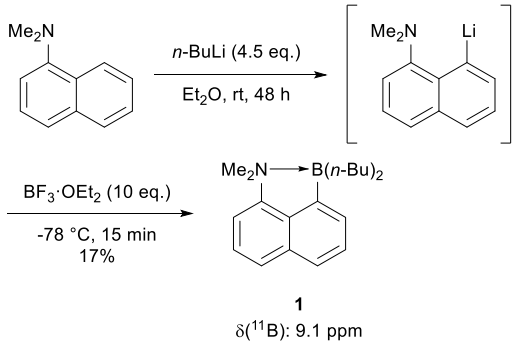

1
δ(^{11}B): 9.1 ppm

Scheme 5 Synthesis of the N-B naphthalene derivative **1**.

Boronic acid derivative **2**[21] (Scheme 6) also displays intramolecular N→B interaction as apparent from its ^{11}B NMR signal at 10.6 ppm which is shifted upfield by 18 ppm with respect to that of 1-naphthaleneboronic acid (28.6 ppm).[22] The strong N→B interaction prevents **2** from undergoing Suzuki-Miyaura coupling reactions. Whatever the conditions used, the boronic acid was recovered unreacted. When the reaction of the lithiated amine with $B(OMe)_3$ was followed by basic instead of acidic work-up, the corresponding boroxine **3** was obtained in 69% isolated yield, as described by Whiting *et al*. in 2003 (Scheme 6).[23] Boroxines are usually planar and aromatic due to delocalization of three O lone pairs over the six-membered ring. In marked contrast, the X-ray diffraction analysis performed on **3** revealed that the amino-naphthyl group forces intramolecular N→B interactions and distorts the central $(BO)_3$ ring from planarity. All three N–B distances are similar (1.902(4) to 1.978(4) Å) and are relatively long compared to the sum of N and B covalent radii (1.55 Å[24], *r* = 1.23 to 1.28) while the B centres are significantly pyramidalized ($\Sigma_\alpha B$ = 348.96°, THC = 45%).

The N→B interaction does not quench reactivity of the B centre in **3** as illustrated by the formation of the corresponding pinacol boronate ester **4** and difluoroborane **5** (Scheme 6). The boron centre of **4** is more Lewis acidic than that of the boroxine **3**, resulting in a stronger intramolecular N→B interaction. This is apparent from the shorter N–B distance (1.832(7) Å, *r* = 1.18) and a more pyramidalized B centre ($\Sigma_\alpha B$ = 342.8°, THC = 59%). Compound **5** is an interesting case that highlights the faculty of the naphthyl scaffold to enforce and strengthen N→B interactions. Accordingly, the reaction with KHF_2 stops at the amine-difluoroborane and the corresponding ammonio trifluoroborate was not formed even under forcing conditions.[9,23] The number of fluorine atoms introduced at boron is easily deduced from the coupling pattern of the ^{11}B NMR signal (triplet in the case of **5** with $^1J_{B\text{-}F}$ = 56.4 Hz). The X-ray structure of **5** was reported recently by Pla, Gras *et al*.[8] The N−B distance is short (1.726(2) Å, *r* = 1.11) and the B centre is highly pyramidalized ($\Sigma_\alpha B$ = 341.8°, THC = 68%). In addition, the naphthyl scaffold distorts to respond the increased Lewis acidity at B and accommodate the strong N→B interaction: the bond angles at the *peri* positions significantly deviate from the ideal value of 120° to 111.55° (N-C_{peri}-C_{bridge}) and 108.99° (B-C_{peri}-C_{bridge}).[9] Calculations by Mebs, Beckmann *et al*. accurately reproduce the N-B bond length in **5** (1.798 Å), and classify this derivative as a regular Lewis pair with an attractive *peri* interaction as determined through a negative α-PIE (-43.6 kJ/mol).[25] Conversely and contrary to experimental results, all attempts to optimize a Lewis pair form with N→B interaction for **4** resulted in an open FLP form. The computed N–B distance is long (2.526 Å) and α-PIE is positive (21.2 kJ/mol).[25] Dispersion effects

and crystal packing are presumed to be responsible for the closed structure observed experimentally.

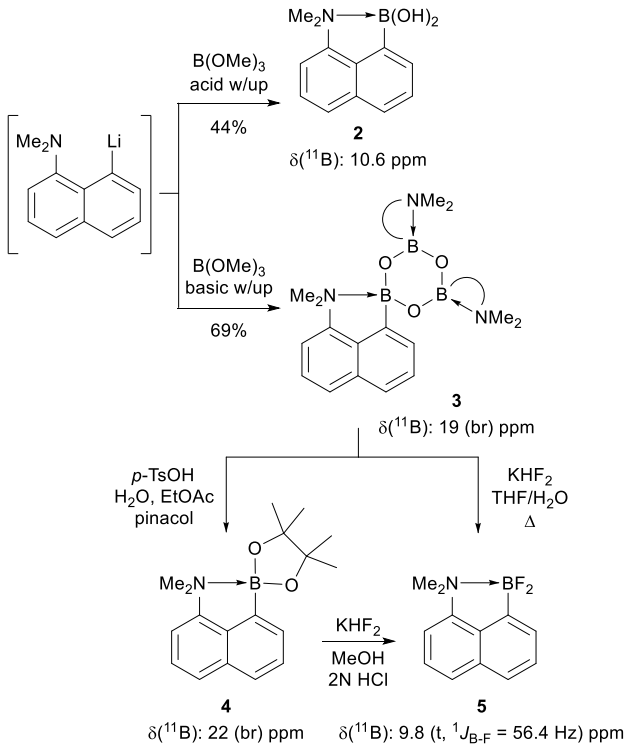

Scheme 6 Synthesis of the boronic acid **2** and boroxine **3**, subsequent reactivity at boron.

The same report by Pla, Gras *et al*. highlighted the importance of the scaffold in enforcing or preventing the formation of intramolecular N→B interactions.[9] Using the more rigid acenaphthyl limits possible distortions in the scaffold and deviations of the *peri* positions from their ideal geometry. This framework maintains N and B at longer distance than the naphthyl backbone, which given the size of the two atoms, prevents the formation of strong N→B interaction. This situation was first exemplified by pinacol derivative **6** (Scheme 7). Its ^{11}B NMR signal is ~10 ppm downfield to that of **4**, the geometry at B remains trigonal planar (Σ_αB = 360°) and the N–B distance (2.773(2) Å) is far away from the sum of covalent radii (*r* = 1.79). The absence of N→B interaction was confirmed computationally: the N–B distance is long (2.855 Å) and α-PIE is positive (26.9 kJ/mol).[25] Contrary to what was observed with the naphthyl scaffold and due to the lack of N→B interaction in the acenaphthyl boronate ester **6**, treatment with KHF_2 gave access to the ammonio trifluoroborate **7**.

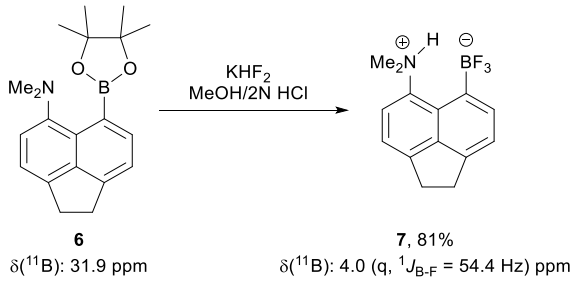

Scheme 7 Structure of the pinacol ester **6** and its conversion into the ammonio trifluoroborate **7**.

Mesityl groups were then introduced at boron to prevent N→B interaction (Scheme 8).[9] They are less electron donating than pinacol, but impart huge steric protection. Derivatives **8** and **9** have downfield ^{11}B chemical shifts, 68.1 and 74.0 ppm, respectively, suggesting trigonal planar B centres

with minimal N→B interactions. This bonding situation is confirmed in the solid state with N–B distances of 2.866(2) Å (*r* = 1.85) and 3.025(2) Å (*r* = 1.95) for **8** and **9**, respectively (the acenaphthalene spacer increases the *peri* distance). The upfield ^{11}B signal of **8**, compared to **9**, is consistent with the significantly shorter N–B distance and is indicative of a very weak N→B interaction. This was corroborated by Natural Bond Orbital (NBO) analyses where calculated D→A interactions show the N→B stabilization energy to be twice as large in **8** than in **9** (8.3 and 4.4 kcal/mol, respectively).[9] Additional calculations by Mebs, Beckmann *et al.* classify both **8** and **9** as FLPs: the N–B distances are well-reproduced (2.992 and 3.095 Å, respectively) and the α-PIE are very positive (33.2 and 31.5 kJ/mol, respectively).[25] The weakness of these interactions explains that the B centre remains about trigonal planar in **8** and **9** (Σ_αB = 358.2 and 358.4°, respectively). Nonetheless, steric congestion causes significant deviations of the *peri* groups from the mean (ace)naphthalene planes. The most significant displacement is the out-of-plane deviation of B (by 0.343 and 0.310 Å for **8** and **9**, respectively).

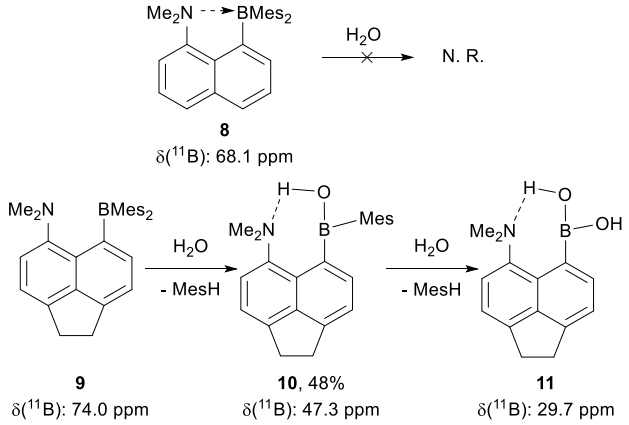

Scheme 8 Structures of the N-$BMes_2$ acenapthalene compounds **8** and **9**, reaction of **9** with H_2O.

Of note, the slight difference in stereoelectronics between **8** and **9** confers drastically different reactivity profiles. While **8** is unreactive towards H_2O, **9** reacts with H_2O in a stepwise fashion to give the borinic acid **10** and finally the boronic acid **11** (Scheme 8)**.** This reaction most likely involves FLP activation of water, resulting in the proto-deboronation of the mesityl groups. The structures of the borinic and boronic acids **10** and **11**, with long N–B distances of 3.140 Å (*r* = 2.03) and 3.170 Å (*r* = 2.05), respectively, further evidence the role of the acenaphthalene scaffold in preventing N→B interactions. Instead, and in contrast to what was observed in the naphthyl boronic acid **2**, compounds **10** and **11** are engaged in intramolecular $Me_2N\cdots H{-}O$ hydrogen bonding.

Steric repulsions at B can be overcome and N→B interaction can be enforced by increasing Lewis acidity at B with electron-withdrawing pentafluorophenyl groups, as shown by Mitzel *et al*.[26] in 2012 with the amine-borane **12** (Chart 3). The upfield ^{11}B NMR signal at 4.8 ppm is indicative of a tetracoordinate and pyramidalized B centre. This is further corroborated by the small separation in chemical shifts between the *m*- and *p*-F signals by ^{19}F NMR spectroscopy ($\Delta\delta^{19}F_{m\text{-}p}$ = 6.6 < 10 ppm).[27] The presence of strong intramolecular N→B interaction in **12** was confirmed crystallographically. The N−B distance is short at 1.742(2) Å (*r* = 1.12) but not as much as in the related unconstrained derivative $Me_2N(CH_2)_3B(C_6F_5)_2$ (1.672(2) A°, *r* = 1.08).[28] The B centre is in a strongly pyramidalized environment (Σ_αB = 337.9°, THC = 63%) while the naphthalene scaffold remains fairly coplanar (C_1-C_9-C_{10}-C_5 torsion angle of 0.77°). Small displacements out of the mean naphthalene plane for N and B (0.140 and 0.203 Å, respectively) enable the substituents at N and B to not be eclipsed and thereby

minimize steric repulsions. The flexibility of the naphthalene scaffold to accommodate the N→B interaction is evidenced by distortions in the *peri* bond angles of 110.6(1)° (B-C_{peri}-C_{bridge}) and 109.6(1)° (N-C_{peri}-C_{bridge}). The strength of this interaction was confirmed by calculations which accurately reproduced the N–B bond length (1.753 Å) and classify **12** as a regular Lewis pair with a very negative α-PIE (-42.7 kJ/mol).[25]

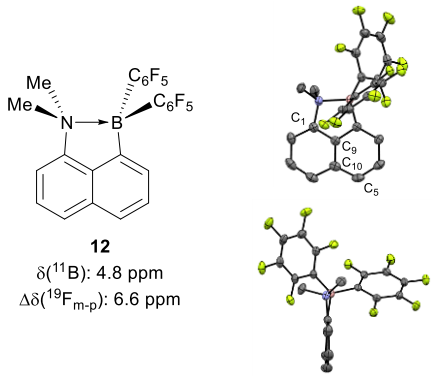

12
$\delta(^{11}B)$: 4.8 ppm
$\Delta\delta(^{19}F_{m\text{-}p})$: 6.6 ppm

Chart 3 Structure of the N-B$(C_6F_5)_2$ derivative **12** (front and side views); carbon in grey, nitrogen in blue, boron in pink, fluorine in green and H atoms omitted for clarity.

Yamamoto, Akiba *et al*. reported in 2002 the only N-B compounds based on an anthracene scaffold, obtained in six steps from commercially available 1,8-dichloroanthroquinone (Scheme 9).[29] As substantiated by X-ray diffraction analyses, only one N atom interacts with B, the other remains at non-bonding distance (> 2.90 Å). Comparison of the structural parameters for the three derivatives revealed significant differences according to the boron Lewis acidity at B: the N–B bond length decreases from 1.809(2) Å for **13**, to 1.739(2) Å for **14**, and 1.664(3) Å for **15**, (*r* = 1.17, 1.12 and 1.07, respectively) while the pyramidalization at B increases (Σ_αB = 346.2, 344.4 and 342.3°; THC = 53%, 55% and 57% for **13**, **14** and **15**, respectively). Thus, despite the rigidity of the anthracene moiety, the N→B interaction responds to the B Lewis acidity and strengthens in the series B(1,2-$O_2C_6H_4$) < BMe_2 < BCl_2.

Given the presence of two equivalent N-donors, a switch of boron from one side to the other was expected to occur. At room temperature, the ^{1}H NMR spectra of all compounds showed symmetrical anthracene patterns, and peaks maintained their sharpness, even upon cooling to -80 °C. These observations indicate that the switch of B between the coordination of either N is rapid on the NMR timescale in solution even at low temperature. The energy barrier associated with this process is too low to be measured. The structure with the two N atoms interacting with B (pentacoordinate, S_N2-type transition state) does not lie much higher in energy than the unsymmetrical tetracoordinate ground-state form.

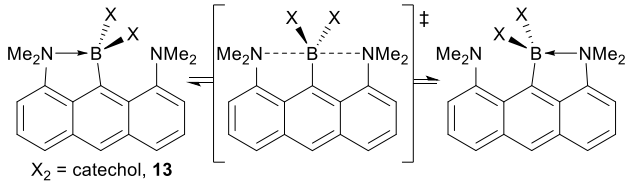

X_2 = catechol, **13**
$\delta(^{11}B)$: 18.5 (br) ppm
X = Me, **14**
$\delta(^{11}B)$: 11 (br) ppm
X = Cl, **15**
$\delta(^{11}B)$: 13.5 (br) ppm

Scheme 9 Anthracene derivatives **13**-**15** and their dynamic equilibrium.

3.2. (Ace)naphthalene N-E[13] derivatives (E[13] = Al, Ga, In, Tl)

In parallel to amine-boranes, the naphthyl scaffold has also been shown to support intramolecular N→E[13] interactions with heavier group 13 elements (Al, Ga, In and Tl). The synthetic route used to access these derivatives parallels that developed for their B homologues. They were prepared by trapping a *peri* lithiated naphthyl amine with an electrophilic $E^{13}Cl_n$ derivative.

Among the first examples were the amine dichloro and dibromo-alanes **16** and **17** reported by Meiler *et al*. in 1998 (Chart 4).[30] ^{27}Al NMR spectroscopic data (δ 129-131 ppm) are consistent with tetracoordinate Al centres, supporting the presence of N→Al interactions. Cowley, Jones *et al*. crystallographically confirmed this bonding situation for **16** in 2000.[31] The N–Al distance (2.016(4) Å) only marginally exceeds the sum of the covalent radii (1.92 Å,[24] *r* = 1.05). It is slightly longer than that observed in the related unconstrained derivative *o*-$(Me_2NCH_2)C_6H_4AlCl_2$ (1.994(2) Å, *r* = 1.04).[30] The Al centre of **16** is noticeably pyramidalized (Σ_αAl = 347.12°, THC = 52%) while the N and Al centres only slightly deviate from the mean naphthyl plane (displacements of 0.208 and 0.107 Å, respectively). Of note, aluminum is generally a stronger Lewis acid than boron towards nitrogen Lewis bases. Combined with the larger size of Al compared to B (by about 43%), this makes the formation of N→E[13] interaction more favoured with Al than with B because bridging the *peri*-positions requires less distortions with Al. This is apparent from the smaller deviations of the N-C_{peri}-C_{bridge} and E^{13}-C_{peri}-C_{bridge} bond angles from the ideal 120° values observed in **16** (116.16 and 107.48°, respectively) than in the corresponding amine dichloroborane **15** (109.45 and 104.47°).

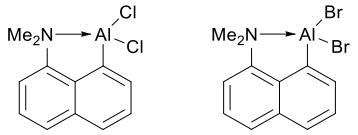

16 δ(^{27}Al): 129 ppm

17 δ(^{27}Al): 131 ppm

Chart 4 Dichloro- and dibromo-alane derivatives **16** and **17**.

Despite the strong N→Al interaction, **16** maintains reactivity at the Al centre. The reaction of **16** with $LiAlH_4$ provided the corresponding aluminum dihydride derivative **18** (Scheme 10).[31] The solid-state structure of **18** shows it to be dimeric and centrosymmetric. The geometry about Al is best described as distorted trigonal bipyramidal with the N and one of the bridging H atoms in axial positions (168.9(2)°). The sum of the angles of the remaining equatorial ligands (H_{bridge}, H and $C_{Naphthyl}$) about Al is 359.7°, indicating coplanarity. The Al–N bond distance in **18** (2.118(3) Å, *r* = 1.10) is slightly longer than that observed in the dichloroalane precursor **16**, in line with reduced Lewis acidity at Al.

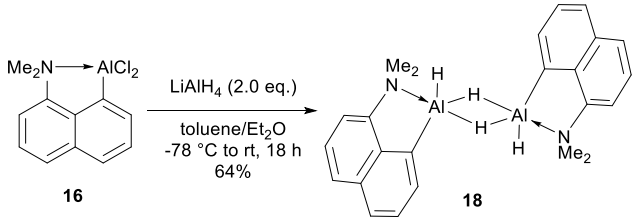

16 **18**

Scheme 10 Reaction of **16** with $LiAlH_4$ to give the aluminum dihydride **18**.

The reaction of **16** with organolithium reagents (MeLi and *t*-BuLi) resulted in redistribution reactions and formation of the bis-naphthyl N-Al-N complexes (**19** and **20**), as established by ^{1}H NMR

spectroscopy, elemental analysis and mass spectrometry (Scheme 11).[31] The dinaphthyl-ethylalane derivative **21** was independently synthesised by Schumann *et al.* in 2004 by reacting two equivalents of 8-lithio-*N,N*-dimethyl-1-naphthylamine with $EtAlCl_2$.[32] The ^{27}Al NMR chemical shift for **21** is significantly upfield (113 ppm), indicative of pentacoordination of the Al centre. In the solid-state structure of **21**, N→Al interactions with larger and slightly different bond lengths (2.244(2) and 2.265(2) Å, *r* = 1.17 and 1.18) were observed. The geometry at Al is an almost perfect trigonal bipyramid, the axial NMe_2 ligands form an angle of 174.62(6)° about Al. However, steric repulsions between the substituents at N and Al force strong out-of-plane deviations (by 0.628 and 0.863 Å for Al, by 0.299 and 0.399 Å for N, the two atoms sitting on opposite sides of the mean naphthyl planes). One naphthyl backbone itself is significantly twisted in the core (torsion angle: 11.49°), while the other remains fairly planar (torsion angle: 4.72°).

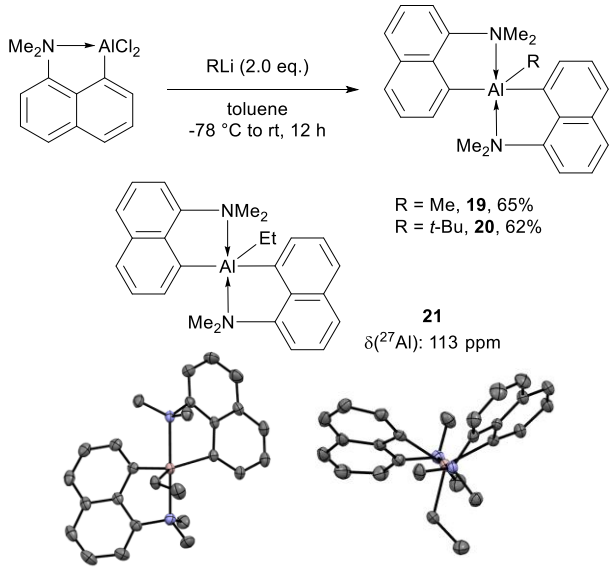

Scheme 11 Synthesis of derivatives **19** and **20** and structure of **21** (front and top views), with carbon in grey, nitrogen in blue, aluminum in pink and H atoms omitted for clarity.

The related N-Al dialkylalanes **22-24** were synthesized by reacting 8-lithio-*N,N*-dimethyl-1-naphthylamine with one equivalent of R_2AlCl (R = Me, Et, *i*-Bu). The observed ^{27}Al NMR chemical shifts are all consistent with tetracoordinate Al centres (Chart 5).[30,32,33] The presence of N→Al interactions was further established by X-ray diffraction analyses in the case of **22** and **23**. The N–Al bond distances are slightly longer than that found in the related dichloro-alane **16**, in line with the reduced Lewis acidity of Al when substituted by alkyl groups. Interestingly, dimethylalane **22** crystallizes with four independent molecules in the unit cell. Two of the four molecules display high planarity with dihedral N-C_{peri}-C_{peri}-Al angles of 0.9 and -2.1°, while the other two molecules are significantly distorted with dihedral angles of 16.8 and -13.9°. These distortions minimize the steric repulsions between the methyl substituents on the Al and N centres, as observed in the planar eclipsed conformation (Chart 5). Overall, there is little variation in the N–Al bond length (ranging from 2.056(2) to 2.070(2) Å, *r* = 1.07 to 1.08) and Al pyramidalization ($\Sigma_\alpha Al$ = 348.5 to 350.5°, THC = 44% to 51%). The molecule has some conformational flexibility, but the N→Al interaction remains about the same. The $AlEt_2$ derivative **23** displays similar behaviour. X-ray diffraction analysis showed little variation in N–Al bond lengths, ranging from 2.068(2) to 2.071(5) Å (*r* = 1.077 to 1.078), and pyramidalization of the Al environment ($\Sigma_\alpha Al$ = 346.6 to 347.9°, THC = 48% to 54%). The N-C_{peri}-C_{peri}-Al torsion angles range from 7.7° to -13.2°, while the naphthalene backbone itself remains fairly

planar. Comparison of the intramolecular N→Al Lewis pair **22** with the corresponding intermolecular (naphthyl)NMe_2→$AlMe_3$ adduct **25**[32] revealed noticeable differences. In the latter compound, the N→Al dative bond is rotated out of the naphthyl plane (Al-N-C_{peri}-C_{bridge} torsion angle = 62.67°) and the N–Al bond length is much longer at 2.157(2) Å (*r* = 1.12) although the Al centre is more pyramidalized (Σ_αAl = 340.3°, THC = 67%) (Chart 5). Bridging the *peri* positions of the naphthyl backbone as in **22** results in a more constrained and shorter N→Al interaction.

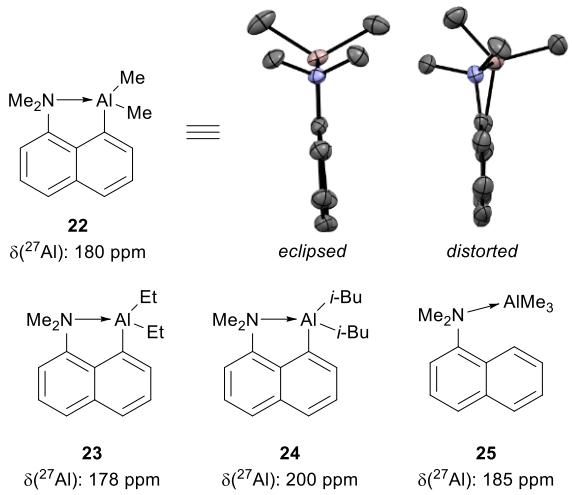

Chart 5 Dialkyl-alane derivatives **22-24** and intermolecular adduct **25**; structure of **22** (two of the molecules found in the unit cell) with carbon in grey, nitrogen in blue, aluminum in pink and H atoms omitted for clarity.

Besides boron and aluminium, a few Ga, In and Tl derivatives featuring 8-dimethylamino-naphthyl substituents were reported.[31,34] The dichlorogalane **26** was obtained as a monomer, while the corresponding indium derivative **27** formed a dimer with bridging Cl ligands (Chart 6). Both compounds were structurally characterised. They are sensitive to air and decompose when exposed to atmosphere. As expected from the similar size and Lewis acidity of Ga as to compared with Al, compound **26** displays strong intramolecular N→Ga interaction. The N–Ga distance in **26** (2.071(7) Å, *r* = 1.07) is slightly longer than the N–Al distance in **16** (2.016(4) Å, *r* = 1.05) and the geometry around Ga is slightly less pyramidalized (Σ_αGa = 349.82°, THC = 42% vs. Σ_αAl = 347.12°, THC = 52%). The N and Ga centres marginally deviate from the naphthalene plane (by 0.168 and 0.09 Å, respectively), resulting in a small N-C_{peri}-C_{peri}-Ga torsion angle of -7.0°. In the solid state, **27** displays a distorted In_2Cl_2 centrosymmetric core with significantly different bridging In–Cl distances, 2.473(2) and 2.746(3) Å. The terminal In–Cl bond lengths are shorter in length (2.352(3) Å). The intramolecular N→In interactions are identical, being 2.406(8) Å (*r* = 1.13) in length, and the geometry at each In centre is best described as trigonal bipyramidal. The axial N and Cl ligands form an angle of 173.0(2)° with In. Small out-of-plane distortions of the N and In centres are observed: 0.072 and 0.183 Å, respectively. In 2012, Beckmann *et al.* reported dinaphthyl substituted In and Tl derivatives **28** and **29** (Chart 6).[34] The two compounds adopt similar dimeric structures in the solid state with bridging Cl ligands. Both In and Tl are six-coordinate and sit in distorted octahedral geometries, with the two naphthyl substituents occupying *trans* positions (C-E^{13}-C bond angles = 158.1(1)° for In and 171.1(3)° for Tl). The N–In (2.550(4)-2.620(5) Å, *r* = 1.20-1.23) and N–Tl (2.701(7)-2.711(6) Å, *r* = 1.250-1.255) bond lengths are very comparable, suggesting N→E^{13} interactions similar in strength with In and Tl. Of note, a single set of ^{1}H and ^{13}C NMR signals was

observed for the NMe_2 groups, suggesting fast E^{13}–Cl dissociation/association on the NMR timescale.

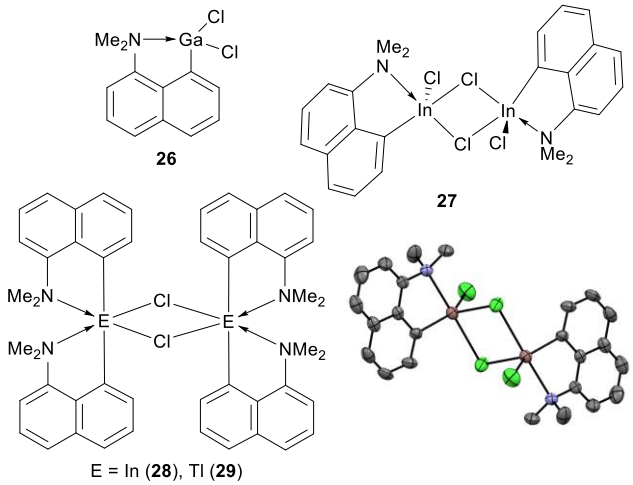

Chart 6 N-Ga, In and Tl derivatives **26**-**29**; structure of **27** with carbon in grey, nitrogen in blue, indium in purple, chlorine in green, and H atoms omitted for clarity.

4.1. (Ace)naphthalene P-B derivatives

The description of (ace)naphthyl supported phosphine-boranes in the literature parallel those of their amine-borane congeners with intensifying research dedicated to these derivatives in the past two decades. The synthetic route used to access these derivatives is similar to that employed for their N homologues, *ie* electrophilic trapping of *peri* lithiated naphthyl phosphines with in some cases Li to Sn transmetalation (*vide infra*).

We described in 2013 a series of naphthyl-bridged phosphine-boranes with varying substituents on the B centre (Chart 7).[35] Both ^{11}B (16.2, 0.1 and -8.5 ppm for **30**, **31** and **32**, respectively) and ^{31}P NMR chemical shifts (17.4, 23.4 and 25.1 ppm for **30**, **31** and **32**, respectively) indicate intramolecular P→B interactions and tetracoordinate B centres. This is confirmed in the solid state with short P–B bond lengths (2.173(4), 2.076(2) and 2.011(2) Å for **30**, **31** and **32**, respectively) that are slightly longer than the sum of P and B covalent radii (1.91 Å[24], *r* = 1.14, 1.07 and 1.05, respectively) and reflect the increasing Lewis acidity at B. The geometry at B is pyramidalized ($\Sigma_\alpha B$ = 341.9(9)°, 340.7(2)° and 338.5(5)°, THC = 39, 60 and 50.4% for **30**, **31** and **32**, respectively). Additionally, the naphthyl scaffold was found to respond to increasing Lewis acidity at B in the order Mes < Cy < fluorenyl through distortions in B-C_{peri}-C_{bridge} *peri* bond angles from the ideal 120° (from 111.4(3)° in **30**, to 109.0(2)° in **32**) as well as P-C_{peri}-C_{peri}-B torsion angles (2.6(2)° to 11.9(2)° for **30** and **32**, respectively). Theoretical calculations are in good agreement with experimental observations,[35] where Natural Population Analysis (NPA) charges indicate electron transfer from P to B with increasing positive and negative charges on P and B, respectively, following the increasing B Lewis acidity (**30**<**31**<**32**). Consistently, the P–B Wiberg bond index (WBI) increases from 0.74 in **30** to 0.88 in **32** and atoms-in-molecules (AIM) calculations show a noticeable increase of the electron density at the P–B bond critical point (BCP) from 0.06 in **30** to 0.10 e.bohr^{-3} in **32**. Of note, a positive α-PIE (39.4 kJ/mol) was computed by Mebs, Beckmann *et al.* for **30**,[25] despite the bonding P→B interaction, which highlights the repulsive interactions induced by the juxtaposition of the bulky (*i*-Pr)$_2$P and $BMes_2$ groups. Contrary to the weak N→B interaction observed with derivative **8**,

strong P→B interactions are enforced despite steric shielding induced by substituents at P and B. The size of P is better suited for the formation of intramolecular P→B interactions without requiring significant distortions of the backbone. The naphthyl scaffold and the P→B interaction retain sufficient flexibility to remain responsive to the Lewis acidity at B.

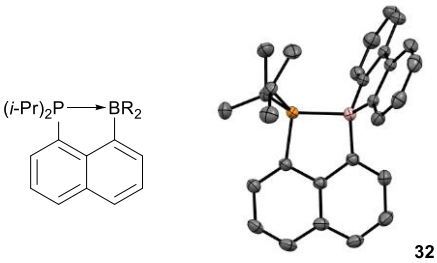

32

	R	$\delta(^{11}B)$	$\delta(^{31}P)$	P-B length (Å)	WBI
30	Mes	16.2	17.4	2.173(4)	0.74
31	Cy	0.1	23.4	2.076(2)	0.81
32	fluorenyl	-8.5	25.1	2.011(2)	0.88

increasing B Lewis acidity

Chart 7 Derivatives **30**-**32** with key analytical data for the P→B interaction; structure of **32** with carbon in grey, boron in pink and phosphorous in orange and H atoms omitted for clarity.

A strong intramolecular P→B interaction is maintained while keeping high steric demand at B and weakening the Lewis basicity of P, as demonstrated by Wang, Beckmann and Mebs, with the Ph_2P-$BMes_2$ derivative **33** (Scheme 12).[36,37] In solution, ^{11}B (13.6 ppm) and ^{31}P NMR data (11.1 ppm) suggest the presence of a P→B interaction and a tetracoordinate B centre. **33** shows six distinct Me signals over the two Mes groups suggesting a highly congested structure, as expected. However, VT ^{1}H and NOESY/EXSY NMR experiments indicate that despite steric congestion, **33** is highly fluxional in solution. The P→B interaction, however, is quite stable. It remains intact, albeit weaker (^{11}B signal shifts from ~15 to ~22 ppm, and ^{31}P signal shifts from ~11 to ~9 ppm), upon heating to 80 °C. The presence of a P→B bond was confirmed in the solid state. The P–B distance is short at 2.1612(16) Å (*r* = 1.13) and the geometry at B is pyramidalized ($\Sigma_\alpha B$ = 346.8°, THC = 37%). The flexibility of the naphthyl scaffold allows it to adapt to the steric congestion imposed by the bulky substituents with significant deviations of the *peri* groups from the mean naphthalene plane (0.278 and 0.275 Å for P and B, respectively). DFT calculations by Wang *et al.*[37] found both the open and closed forms of **33** as minima on the potential energy surface. In the open form, the P–B distance is 3.00 Å, with the lone pair on P still pointing towards B, while the closed form was found to have a P–B length of 2.23 Å. In agreement with experimental observations, the open form was found more stable computationally, but the two forms are very close in energy (ΔE = 4.43 kJ/mol) with an accessible transition state (5.28 kJ/mol), suggesting rapid interconversion. Comparable α-PIE values were computed by Mebs, Beckmann *et al.* for the two forms (30.7 and 34.4 kJ/mol for the closed and open forms, respectively).[25] The presence of the Ph_2P and $BMes_2$ groups in the *peri* positions is overall repulsive, irrespective of the presence, or not, of a bonding P→B interaction.

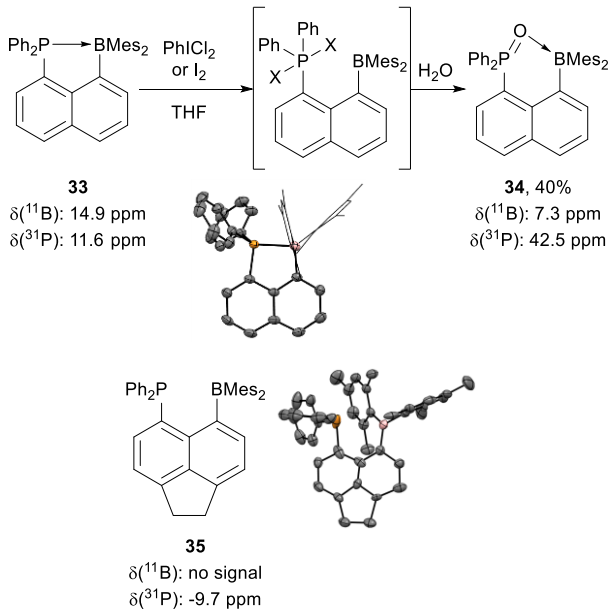

Scheme 12 Oxidation of **33** to **34** and corresponding acenaphthyl-bridged derivative **35**; structures of **33** (Mes groups simplified) and **35** with carbon in grey, phosphorus in orange, boron in pink and H atoms omitted for clarity.

Although involved in an intramolecular P→B interaction, the P centre of **33** maintains reactivity, as exemplified by its reaction with I_2 or $PhICl_2$ to give the phosphineoxide-borane **34** (Scheme 12).[37] This is thought to occur through initial oxidation of P to the halo phosphorane species which then hydrolyses to **34**. The ^{31}P chemical shift (42.5 ppm) is highly indicative of oxidation of P and the ^{11}B chemical shift (7.3 ppm) indicates a tetracoordinate B centre. **34** was characterized in the solid state, finding P=O and O–B bond lengths of 1.532(3) and 1.621(6) Å, respectively, while the geometry about B is highly pyramidalized ($\Sigma_\alpha B$ = 342.0(4)°, THC = 68%).

In line with that discussed in the previous section on N→E[13] derivatives, the acenaphthyl scaffold can be used to disrupt *peri* interactions. This is also the case with phosphine-borane **35** (Scheme 12).[36] While a ^{11}B NMR signal could not be observed, the ^{31}P NMR chemical shift (-9.7 ppm) is indicative of the lack of intramolecular P→B interaction. This bonding situation was confirmed in the solid state, with a long P–B distance of 3.050(3) Å (*r* = 1.60) and trigonal planar geometry at B ($\Sigma_\alpha B$ = 358.4°), classifying **35** as a FLP. Despite increased *peri* distances, **35** still experiences significant deviations of both *peri* groups from the mean acenaphthalene plane (0.129 and 0.456 Å for P and B, respectively). Theoretical calculations compared real-space bonding indicators (RSBIs) between **33** and **35**. All RSBIs could clearly discriminate bonding and non-bonding P–B contacts in **33** and **35**, respectively. This is attributed to the enhanced rigidity of the acenaphthyl backbone, compared to the naphthyl framework which is flexible enough to allow shorter *peri* interactions. Of note, the α-PIE calculated for the FLP **35** (30.2 kJ/mol)[25] is very similar to those of the open and closed forms of **33**, indicating that the nature of the backbone, acenaphthyl or naphthyl, has little overall impact on the repulsive interactions generated by the juxtaposition of the Ph_2P and $BMes_2$ groups.

This effect of the rigid acenaphthene backbone was also exemplified very recently by Beckmann *et al.* in related boronic esters **36** and **37** (Scheme 13).[38] **36** was found to be sensitive to water and hydrolyses to the corresponding boronic acid **38**. Subjected to elevated temperatures and reduced pressure, **38** is prone to condensation and forms the corresponding boroxine **39**, which while relatively stable undergoes slow oxidation at one P-site to yield boroxine **40**. As opposed to N→B

boronic acid **2** and boroxine **3**, the acenaphthene framework here prevents the formation of any P→B interactions. All these derivates show spectroscopic signatures of tricoordinate B centres (downfield ^{11}B NMR chemical shifts) and lack of P→B interactions (upfield ^{31}P NMR chemical shifts). These bonding situations were confirmed in the solid-state, finding long P–B distances for **36**-**40** (>2.762 Å, *r* > 1.5) and trigonal planar B centres. Despite the lack of P→B interactions, these derivatives were found to be inert towards Suzuki-Miyaura cross-coupling reactions.

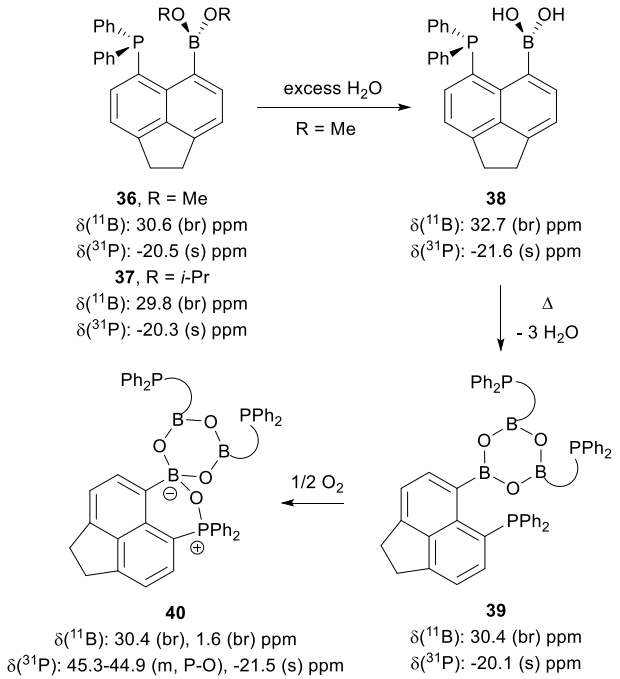

Scheme 13 Hydrolysis of **36** into **38** and formation of boroxines **39** and **40**.

The rigidity of the acenaphthalene scaffold can be overcome and the formation of P→B interactions promoted by increasing the Lewis acidity at B, as demonstrated by Mebs, Chęcińska and Beckmann with phosphine-boranes **41**-**45** (Scheme 14).[25,39] Transmetalation of (6-diphenylphosphinoacenaphth-5-yl)tributylstannane with $Me_2S{\cdot}BH_3$ provided the phosphine-borane **41** with the smallest boryl site, as a reasonably air-stable solid. Through redistribution, **41** reacted with tris(pentafluorophenyl)borane to provide **42** (sensitive to air and moisture) which could be chlorinated with SO_2Cl_2 to give the corresponding chloroborane **43**. While a second pentafluorophenyl substituent could not be introduced from **43**, the bis(pentafluorophenyl)borane **44** was independently synthesised by directly trapping (6-diphenylphosphinoacenaphth-5-yl)lithium with $ClB(C_6F_5)_2$, to provide **44** as an air stable solid.

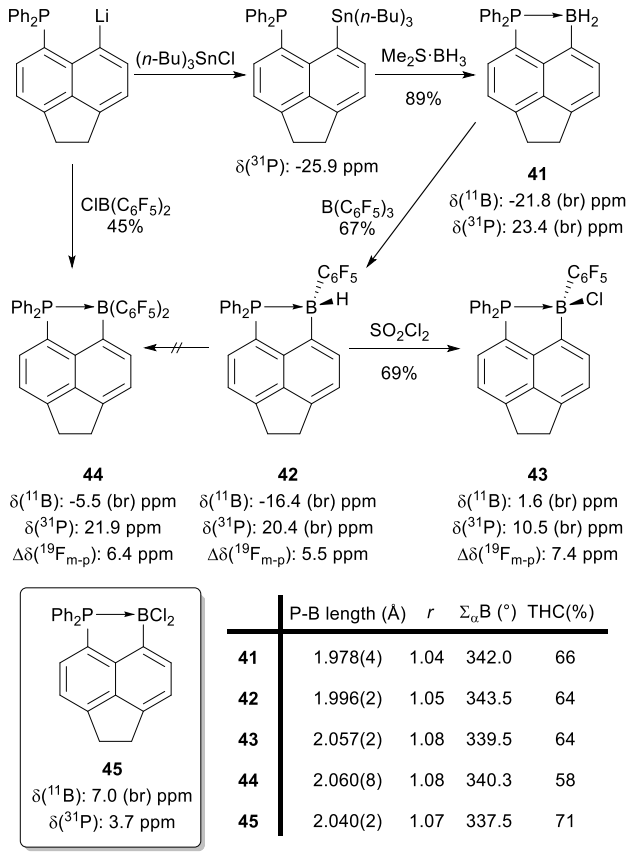

	P-B length (Å)	*r*	Σ_αB (°)	THC(%)
41	1.978(4)	1.04	342.0	66
42	1.996(2)	1.05	343.5	64
43	2.057(2)	1.08	339.5	64
44	2.060(8)	1.08	340.3	58
45	2.040(2)	1.07	337.5	71

Scheme 14 P-B acenaphthalene derivatives with highly Lewis acidic B centers **41**-**45**.

All derivatives **41**-**45** show spectroscopic evidence of intramolecular P→B interactions and tetracoordinate B centres, as apparent from upfield ^{11}B and downfield ^{31}P NMR signals. This is further evidenced in C_6F_5-containing derivatives **42**-**44** by small separations in chemical shifts between the ^{19}F NMR *m*- and *p*-F signals ($\Delta\delta^{19}F_{m\text{-}p}$ = 5.5, 7.4 and 6.4 ppm for **42**, **43** and **44**, respectively).[27] These bonding situations were confirmed in the solid state with short P–B bond lengths and pyramidalized B centres (see table in Scheme 14). Despite its rigidity, the acenaphthyl scaffold responds to the Lewis acidity at B through distortions from the ideal 120° in *peri* bond angles (up to 107.10° for P-C_{peri}-C_{bridge} and 113.45° for B-C_{peri}-C_{bridge}), while the core acenaphthyl scaffold itself remains fairly coplanar. Theoretical calculations supported these findings, with no open or FLP structures found as minima on potential energy surfaces for any of these derivatives. **41**-**45** were all classified as regular Lewis pairs with overall attractive *peri* interactions (negative α-PIE of -80.3, -84.6, -45.3, -51.6 and -43.8 kJ/mol were computed for **41**, **42**, **43**, **44** and **45**, respectively). In addition, topological analyses (AIM calculations) of the P–B bonding show in all cases high degree of covalency.[25]

Formation of P→B interactions is highly sensitive to steric congestion at B centres as well as the donating ability of P, as demonstrated by Sasamori, Tokitoh *et al*. with the dichlorophosphine-boranes **46a**-**48a** (Scheme 15).[40] Placement of bulky *t*-Bu groups in *meta* positions of the Ar groups in **46a** allows formation of a P→B interaction and a tetracoordinate B centre, as demonstrated by an upfield ^{11}B NMR signal at 10 ppm. However, di-*ortho* substituents Ar prevent P→B interactions in **47a** and **48a** and maintain tricoordinate B centres (evidenced by downfield ^{11}B NMR signals of 63.9 and 64.3 ppm, respectively). These bonding situations were confirmed in the solid state, finding a short P–B contact for **46a** (2.108(2) Å, *r* = 1.10) but a long P–B distance in **47a** (2.961(2) Å, *r* =

1.55).[41] Calculations accurately reproduce the long P–B distance in **47a** (2.912 Å) and classify this derivative as a FLP with a positive α-PIE (12.9 kJ/mol).[25]

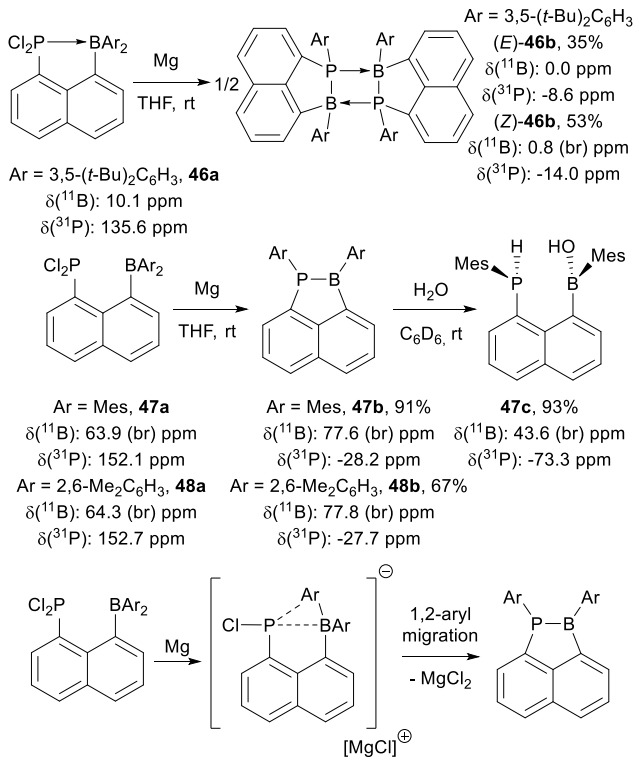

Scheme 15 Reduction of the Cl_2P-B naphthyl derivatives **46a**-**48a** to give **46b**-**48b**, activation of H_2O by **47b** to give **47c**, and proposed mechanism of reductive 1,2-aryl migration.

These derivatives displayed unique reactivity under reducing conditions (with Mg) involving the formation of a P–B bond and 1,2-aryl migration to give the corresponding 1-phospha-2-boraacenaphthenes **46b**-**48b** (Scheme 15). Due to reduced steric congestion about the B centre in **46a**, head-to-tail dimerization occurs to provide the dimeric product **46b** as a mixture of *E* (35%) and *Z* (53%) isomers with tetracoordinate B centres, as suggested by ^{11}B NMR spectroscopy (0.0 and 0.8 ppm for *E* and *Z* isomers, respectively). Conversely, reduction of **47a** and **48a** provides the corresponding 1-phospha-2-boraacenaphthenes **47b** and **48b** as monomers. Here, head-to-tail dimerization is prevented by steric congestion at the B centres. Tricoordinate B centres are evidenced by downfield ^{11}B NMR signals (77.6 and 77.8 ppm for **47b** and **48b**, respectively) while upfield ^{31}P NMR signals (-28.2 and -27.7 ppm for **47b** and **48b**, respectively) support monomeric structures. This was further confirmed crystallographically for **47b**, finding a trigonal planar B centre (Σ_αB = 359.5(6)°) and a very short P–B bond (1.889(3) Å, *r* = 0.99). The P centre is pyramidalized (Σ_αP = 328.4(3)°) and deviates significantly from the mean naphthalene plane (0.356 Å). This structural arrangement does not allow for π(PB)-bonding (donation of the lone pair on P into the vacant 2p orbital on B). sp^2 hybridization of P is energetically demanding so that the lone pair at P retains high s character and hardly overlaps with the vacant 2p(B) orbital.

The presence of proximal Lewis basic and acid sites allows **47b** to activate H_2O in a FLP-like fashion to afford 1-hydroxy(mesityl)boryl-8-mesitylphosphinonaphthalene **47c** in excellent yield, representing the formal addition of H_2O across the P–B bond. No P→B interaction is observed in **47c** as shown by the downfield ^{11}B (43.6 ppm) and upfield ^{31}P NMR signals (-73.3 ppm) (Scheme 15).[40] **47b** also demonstrated reactivity in chalcogenation reactions with S_8

and Se to give derivatives **49**-**53** (Scheme 16).[41] The P–B bond is broken in all derivatives to accommodate the newly formed P-S(Se)-B motif and the P atom is eventually oxidized to the corresponding sulfide or selenide, leaving tricoordinate B centres, as evidenced by downfield ^{11}B NMR signals. This was unambiguously verified in the solid state, with long P–B distances (> 3 Å, *r* > 1.60) and trigonal planar B centres (Σ_αB = 360°) for **49**-**53**.

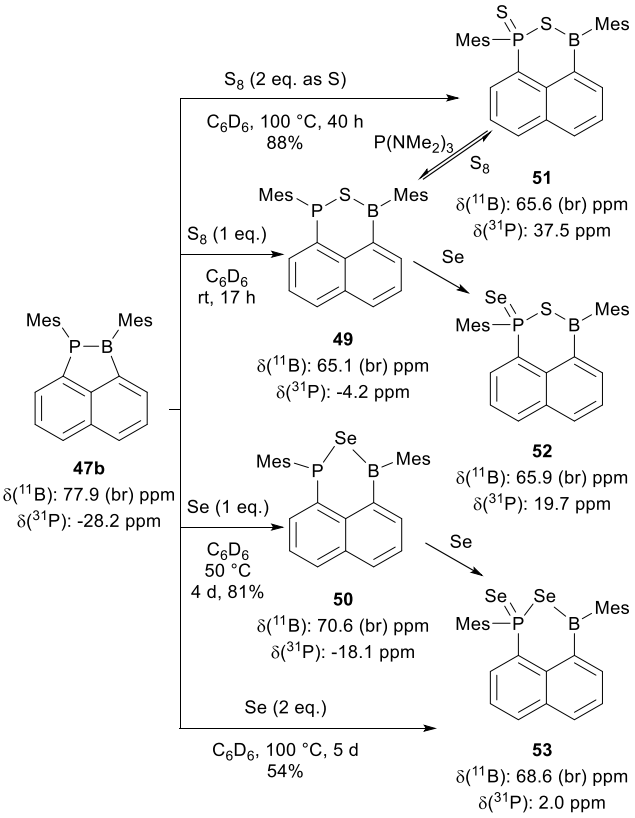

Scheme 16 Chalcogenation reactions of **47b**.

Related to their work on anthracene-bridged N-B-N derivatives (**13**-**15**), Yamamoto, Akiba *et al*. reported in 2001 an analogous system **54** using P(*i*-Pr)$_2$ as the Lewis base (Scheme 17).[42] It was obtained in six steps from 1,8-dichloroanthraquinone. In solution, ^{11}B NMR spectroscopy (15.0-25.0 ppm) suggests a weak P→B interaction. This is verified in the solid state, and as observed with the N-B-N derivatives **13**-**15**, only one P atom interacts with B (2.15 Å, *r* = 1.13). The other remains at a long non-bonding distance (3.17(3) Å) and the geometry at B is slightly pyramidalized (Σ_αB = 345.6°, THC = 55%). Only very slight distortions in *peri* bond angles from the ideal 120° are observed in **54** (112.5°-114.8°) compared to the N-analogues **13**-**15** previously described (104.5°-111.6°). Given the presence of two equivalent P-donors, a switch of boron from one side to the other was expected. At room temperature, the ^{1}H NMR spectrum showed a symmetrical anthracene pattern, and peaks maintained their sharpness, even upon cooling to -80 °C. These observations indicate that the switch of B between the coordination of either P is also rapid at the NMR timescale in solution, even at low temperature. The energy barrier associated with this process is too low to be measured.

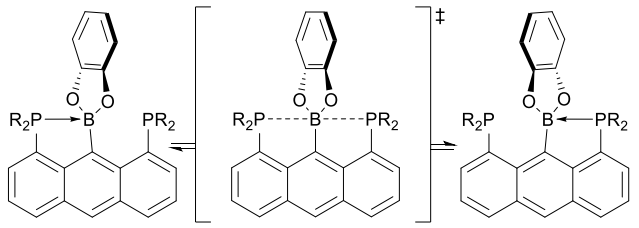

Scheme 17 P-B-P Anthracene derivative **54** and its dynamic equilibrium.

4.2. (Ace)naphthalene P-E^{13} derivatives (E^{13} = Al, Ga, In, Tl)

Mirroring contributions and reports on N→E^{13} derivatives previously discussed, P→E^{13} interactions have also been extended to heavier group 13 elements (E^{13} = Al, Ga, In and Tl) using the acenaphthalene scaffold, as reported by Chęcińska, Beckmann *et al*. (Chart 8).[39] Access to these derivatives is generally achieved by Li to Sn transmetalation and reaction of (6-diphenylphosphinoacenaphth-5-yl)tributylstannane with the desired E^{13}Cl$_n$ reagent. Mono-, di- and trisubstituted alanes **55**-**57** could only be obtained by reacting $AlCl_3$ with (6-diphenylphosphinoacenaphth-5-yl)lithium (no reactivity with the tin derivative) while varying the stoichiometry and order of addition of reactants. These derivatives are sensitive and decompose immediately upon exposure to moist air. Their structures were confirmed in the solid state. Compound **55** displays a short P–Al bond (2.4305(6) Å) which is slightly longer than the sum of P and Al covalent radii (2.28 Å, *r* = 1.07). The Al centre is only slightly pyramidalized (Σ_αAl = 346.77°, THC = 47%). Both **56** and **57** display elongated P–Al bonds with small variations in each derivative (2.6934(7) and 2.7405(7) Å, *r* = 1.18 and 1.20 for **56**, and 2.831(1), 2.909(1) and 2.943(2) Å, *r* = 1.24, 1.28 and 1.29 for **57**). The geometry at Al in **56** is best described as trigonal bipyramidal. The axial P ligands form an angle of 170.96(2)° with Al, and the third equatorial position is occupied by Cl (Al–Cl bond length: 2.1658(7) Å). In **57**, the Al centre adopts a distorted octahedral geometry with a *facial* arrangement of the (P,C) ligands. Expectedly, due to similar size and Lewis acidity of Ga as to compared with Al, dichlorogalane **58** displays a strong intramolecular P→Ga interaction. The P–Ga distance in **58** (2.411(2) Å, *r* = 1.05) is marginally shorter than the P–Al distance in **55** (2.4305(6) Å, *r* = 1.07) and the geometry around Ga is similarly pyramidalized (Σ_αGa = 345.78°, THC = 48%). In the solid state, **59** displays analogous geometry to its NMe_2-analogue **27**, with a distorted In_2Cl_2 centrosymmetric core and significantly different bridging In–Cl distances (2.4429(4) and 2.7855(5) Å). The intramolecular P→In interactions are identical being 2.7042(5) Å (*r* = 1.09) in length and the geometry at each In centre is best described as trigonal bipyramidal. The axial P and Cl ligands form an angle of 168.96(1)° with In. In the solid state, the Tl derivative **60** displays a short P–Tl bond (2.7726(6) Å, *r* = 1.10) and the geometry at Tl is planar (Σ_αTl = 359.12°). Calculated RSBIs identify derivatives **55**-**60** as regular Lewis pairs with attractive *peri* interactions. The P→Al interaction of **55** shows the highest degree of ionicity (based on electron density RSBIs derived from AIM and electron localizability indicator (ELI-D) parameters). Calculations did not find any minima on potential energy surfaces corresponding to open/FLP structures of **55**-**60**, highlighting that the size and diffuse nature of P and the electronic character of heavier group 13 elements match very well and combine in a synergistic fashion resulting in strong P→E^{13} interactions.

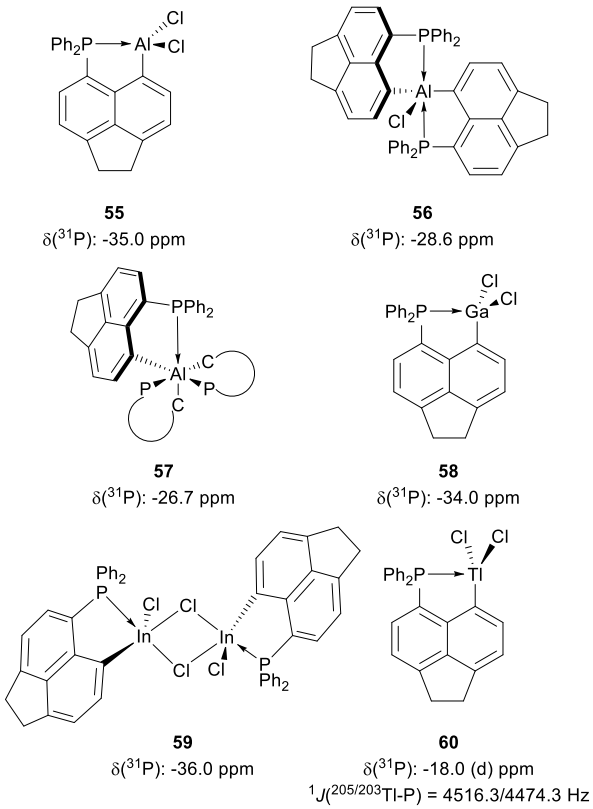

Chart 8 Acenaphthalene-bridged P→E[13] derivatives **55**-**60**.

5.1. P-stabilised borenium cations

Considering the propensity of the naphthyl backbone to enforce strong intramolecular P→B interactions, our group investigated the ability of these systems to stabilise borenium cations, as surrogates for electron deficient boranes. Our synthetic strategy begins with classical formation of neutral P-B adducts starting from lithiation of the 1-iodo-8-phosphinonaphthalene followed by trapping with a dibromoborane to furnish bromoboranes **61**-**63** with varying donating ability of the P centre (Scheme 18).[43–45] Notably, derivative **63** is a rare example of a stable and isolable phosphine-borane with an alkyl substituent on B. The cyclohexyl group is a weaker donor compared to Mes and previously described aromatic substituents. In line with related phosphine-boranes, the naphthyl scaffold enforces strong intramolecular P→B interactions resulting in tetracoordinate B centres, as evidenced by upfield ^{11}B (0.3, -1.5 and 2.0 ppm for **61**, **62** and **63**, respectively) and downfield ^{31}P NMR signals (1.8, 14.1 and 16.4 ppm for **61**, **62** and **63**, respectively). This bonding situation was confirmed in the solid state for **61** and **63**, finding short P–B bond lengths (2.05(1) and 2.021(3) Å, *r* = 1.07 and 1.06, respectively) and strongly pyramidalized B centres (Σ_αB = 339.4 and 336.8°, THC = 58 and 65%, respectively). Here again, the flexibility of the naphthyl scaffold accommodates steric congestion in **61** through significant deviations of the *peri* groups from the mean naphthalene plane (0.332 and 0.235 Å for P and B, respectively), as well as significant distortions from ideal *peri* bond angles of 120° (<117° in both **61** and **63**). Calculations accurately reproduced the short P–B bond length observed in **61** (2.071 Å) and classify this derivative as a regular Lewis pair with attractive *peri* interactions (negative α-PIE of -25.6 kJ/mol).[25]

The corresponding borenium cations could then be formed by abstracting the Br atom from B using $GaBr_3$ or $AgNTf_2$ as dual-purpose Br scavengers and counteranion sources (Scheme 18). All borenium cations **64**-**68** display spectroscopic hallmarks of tricoordinate B centres supported by significantly

downfield shifted ^{11}B NMR signals (71.4-77.9 ppm). Stronger P lone-pair donation to B, responding to increased electrophilicity upon cationisation, is indicated by an upfield shift of the ^{31}P NMR signals for **65**, **66** and **68** (19.2, 21.4 and 19.3 ppm, respectively). This was confirmed in the solid state for borenium tetrabromogallates **65** and **66**, with very short P–B distances (1.997(6) and 2.004(4) Å, *r* = 1.045 and 1.049, respectively) and trigonal planar B centres (Σ_αB = 359.4 and 360.0°, respectively). Considering these structural parameters, the bonding situation in these borenium cations is best described as a combination of two canonical or mesomeric structures: a phosphine-stabilised borenium cation and a phosphonio-borane form (Scheme 18). Importantly, these derivatives represent a departure from previously reported borenium cations stabilised by Lewis bases incorporating N (amines or pyridines) or C (NHCs, NHOs or carbodiphosphoranes) donors. They are scarce examples of P-stabilised borenium cations, which had been previously limited to a few intermolecular [(R_3P)→Bcat]$^+$ adducts.[46]

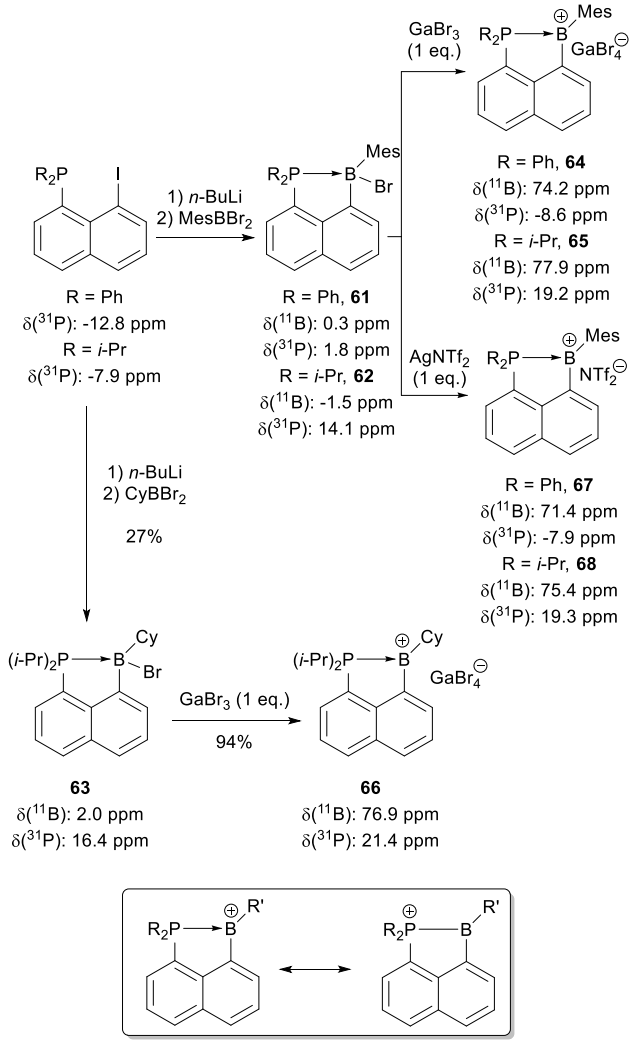

Scheme 18 Synthesis of the naphthyl-bridged phosphine-bromoboranes **61**-**63** and corresponding P-stabilised borenium cations **64**-**68**.

The reactivity of these borenium cations was then investigated with respect to small molecule activation. Borenium bistriflimide **67** was found to form a FLP with *t*-Bu_3P, due to steric congestion, and could activate H_2 with quantitative conversion of the borenium into the corresponding phosphine-hydroborane **69** over 39 hours at room temperature (Scheme 19).[43] ^{31}P NMR monitoring shows the apparition of a new signal at *δ* 11.2 ppm attributed to **69** and a signal at *δ* 56.7 ppm

corresponding to *t*-Bu_3PH^+. The ^{11}B NMR chemical shift of **69** at -13.3 ppm suggests a tetracoordinate B centre. Remarkably, borenium **67** was also found to react with H_2 in the absence of an external base (Scheme 19). Under more forcing conditions, and without an external base, a new derivative **70** is formed quantitatively along with mesitylene. The presence of a P→B interaction and tetracoordinate B centre is apparent from the low field ^{11}B (-6.4 ppm) and high field ^{31}P NMR signals (4.7 ppm). This bonding situation is confirmed in the solid state, finding a very short P–B bond (1.982(3) Å, *r* = 1.04) and a pyramidalized B centre ($\Sigma_\alpha B$ = 336°, THC = 66%) due to coordination of the NTf_2 anion to B (B–N bond length 1.602(4) Å). Mechanistic studies using D_2 shows formation of the deuterated analogue of **70** (^{31}P 4.8 ppm) along with deuterated mesitylene (Scheme 19). DFT studies were employed to elucidate the reaction mechanism. Accordingly, the reaction is proposed to involve side-on coordination of H_2 to B, akin to transition metals, followed by heterolytic cleavage of H_2 and concomitant transfer of a hydride to the B centre and protonation of the Mes substituent. This represents a rare example of heterolytic H_2 activation at a unique non-metallic reactive site.

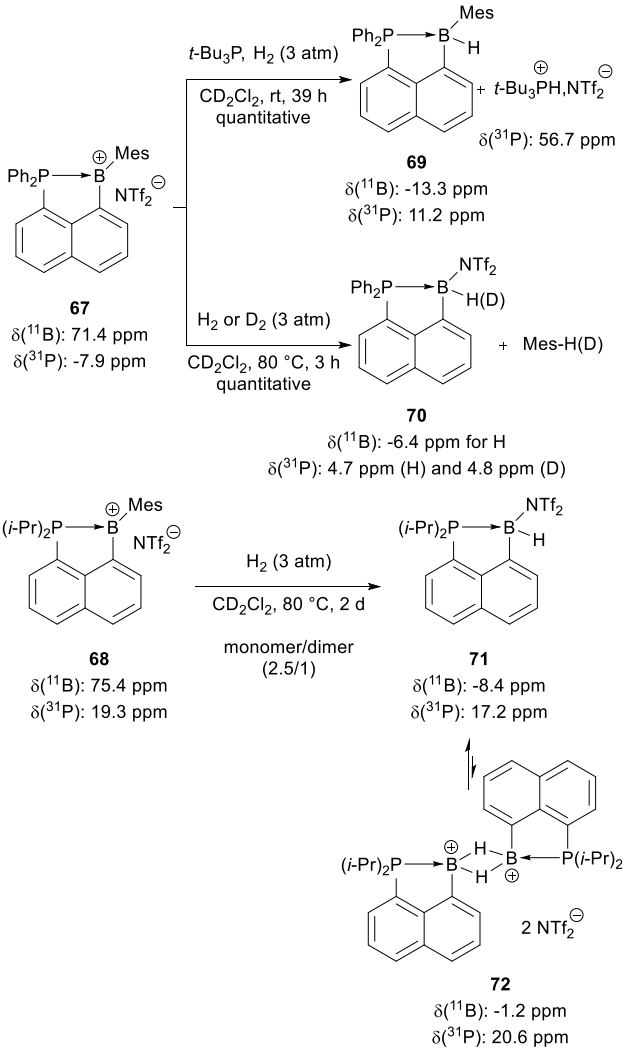

Scheme 19 Activation of H_2 by **67** and **68**.

Similar reactivity was observed with borenium **68**.[44] In this case however, longer reaction times were required (48 h vs. 3 h for **67**) due to stronger donation of the (*i*-Pr)$_2$P moiety to B, decreasing the B electron-deficiency (Scheme 19). The reaction with H_2 provides a mixture of two spectroscopically similar compounds in a 2.5/1 ratio attributed to the phosphine-hydroborane monomer **71** and the

corresponding dicationic dimer **72**. The high field ^{11}B (-8.4 and -1.2 ppm for **71** and **72**, respectively) and low field ^{31}P NMR signals (17.2 and 20.6 ppm for **71** and **72**, respectively) are indicative of strong P→B interactions and tetracoordinate B centres. The bonding situation in **71** was unambiguously determined in the solid state with a short P–B bond length (2.000(4) Å, *r* = 1.05) and a pyramidalized B centre (Σ_αB = 334.6°, THC = 60%) with coordination of NTf_2 to B. Dimerisation is only observed with the $(i\text{-Pr})_2$P derivative (only the monomeric covalent form is observed with Ph_2P), and is thought to be the result of stronger donating ability and higher steric demand of the phosphino group which in turn results in a less Lewis acidic B centre in **71** (compared to **70**) making NTf_2 dissociation and formation of the 2-electron 3-centre B-H bridging interactions more favourable. These studies serve to highlight the effects of remote modulation of Lewis acidity at B by varying the substituents on the P centre.

Besides the ability to activate H_2, the high Lewis acidity of **64**, coupled with the propensity of Mes to fix a proton, allow activation of N–H bonds, as substantiated by its reactivity with diphenylamine (Ph_2NH) to provide the corresponding amino borenium salt **73** (Scheme 20). The ^{11}B NMR signal (42.2 ppm) suggests a tricoordinate B centre, which is 32 ppm upfield from **64** due to π-donation by the amino substituent. This bonding situation was confirmed in the solid state, evidenced by a short P–B bond (1.972(2) Å, *r* = 1.03) as well as a short N–B bond (1.381(8) Å, *r* = 1.55) indicative of double bond character. The geometry at B is trigonal planar (Σ_αB = 359.9°). This reaction is thought to occur in two steps: coordination of the amine to B, then elimination of Mes-H through intramolecular aminolysis of the B–Mes bond.

Seeking to characterize the presumed intermediate of this aminolysis reaction, we reacted **67** with NH_3 as a less acidic analogue of Ph_2NH. When **67** was treated with a NH_3 atmosphere, the corresponding aminoborane **74** was obtained, with retention of the Mes group on B (Scheme 20). The ^{11}B NMR signal (40.4 ppm) is characteristic of a tricoordinate B centre with a 31 ppm upfield shift compared to **67** due to π-donation from NH_2. The lack of a P→B interaction is supported by an upfield ^{31}P NMR signal (-12.6 ppm). This is confirmed in the solid state. The P–B distance (2.971(2) Å, *r* = 1.56) is long while the N–B bond is short (1.390(3) Å, *r* = 0.90) suggesting double bond character. The geometry at B is trigonal planar (Σ_αB = 359.03°). Interestingly, reacting **67** with only one equivalent of NH_3 allows formation of the corresponding boronium salt **75** (Scheme 20). The shifts of the ^{11}B (highfield, at -2.1 ppm) and ^{31}P NMR signals (downfield, at 3.9 ppm) are diagnostic of a tetracoordinate B centre and P→B interaction. This was confirmed in the solid state with a short P–B bond length (2.047(6) Å, *r* = 1.07) and a longer N–B bond (1.602(8) Å, *r* = 1.03) indicative of single bond character. The geometry about B is pyramidalized (Σ_αB = 340.19°, THC = 57%). **74** and **75** can be interconverted by removing or adding excess ammonia to solutions of both derivatives.

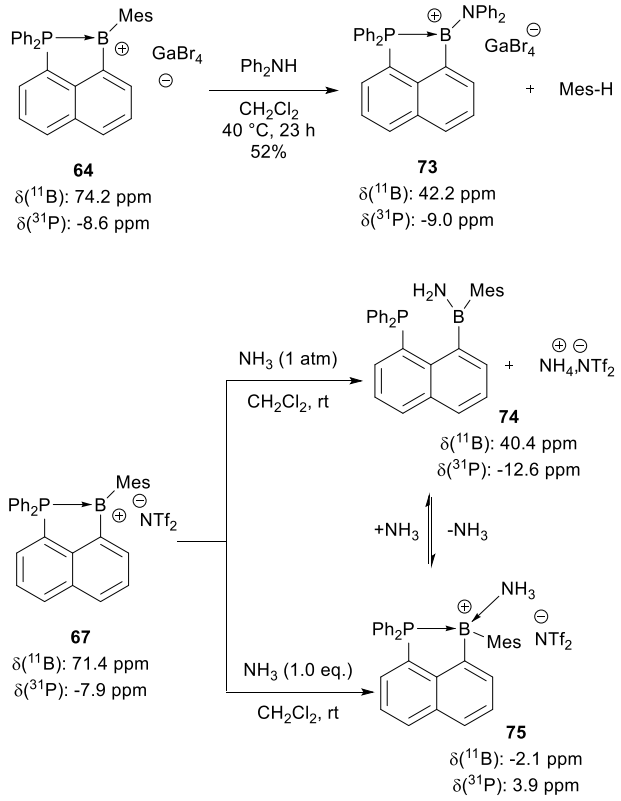

Scheme 20 Reaction of **64** with Ph_2NH (substituent exchange at a borenium center), and reactivity of **67** with NH_3 (coordination of N and N–H bond activation).

Additionally, the reactivity of **64** with more acidic N-H compounds could be leveraged by reacting $HNTf_2$ in the presence of two equivalents of $Et_3P(O)$ to access **76**, a rare example of a stable and isolable dicationic boron compound (Scheme 21). The highly upfield ^{11}B NMR signal (8.6 ppm) suggests a tetracoordinate B centre while the ^{31}P NMR signal at -8.7 ppm evidences the persistence of the P→B interaction. The highly downfield shifted ^{31}P NMR signal attributed to $(O)PEt_3$ (90.8 ppm) indicates the strength of the O→B interactions, due to the high Lewis acidity of the dicationic B centre.

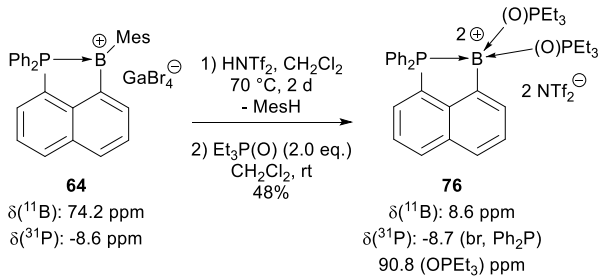

Scheme 21 Formation of the dicationic boron compound **76**.

Our group has also developed an alternative synthesis to amino borenium salts. It starts by the installation of a chloro(diisopropylamino)boryl moiety on the naphthyl phosphine to give **77a** (Scheme 22).[45] In C_6D_6 as solvent, the downfield ^{11}B NMR signal (33.3 ppm) suggests a tricoordinate B centre and the upfield ^{31}P NMR signal (-11.8 ppm), which is similar to that of the parent compound, was indicative of the lack of P→B interaction. This is most likely the effect of strong N→B π-donation effectively decreasing the B Lewis acidity. However, in a more polar solvent, such as $CDCl_3$, the ^{31}P NMR signal moves downfield to 11.3 ppm, while the ^{11}B NMR signal remains downfield at 37.9 ppm,

suggesting the dissociation of Cl from B and concomitant formation of an intramolecular P→B interaction to stabilise the borenium salt form **77b**. This was supported by DFT calculations taking solvent into account using the PCM model, finding that **77a** is more stable than **77b** in benzene ($\Delta E_{\mathbf{77a \rightarrow 77b}}$ = 4.9 kcal/mol), while **77b** is slightly more stable than **77a** in $CHCl_3$ ($\Delta E_{\mathbf{77a \rightarrow 77b}}$ = -0.8 kcal/mol). The bonding situation in **77a** was confirmed in the solid state, with a long P–B distance (2.867(2) Å, *r* = 1.50) and a trigonal planar B centre ($\Sigma_\alpha B$ = 359.7°). In turn, the N–B bond length is short (1.385(3) Å, *r* = 0.89) indicating double bond character.

The nature of **77b** as a borenium salt was confirmed by independent synthesis of borenium salt **78** through irreversible abstraction of Cl from B with $GaCl_3$. The salts **77b** and **78** present nearly identical spectroscopic data, suggesting a tricoordinate B centre and a P→B interaction (both the ^{11}B and ^{31}P NMR signals shift downfield to 37.9 and 13.0 ppm, respectively). The structure of the borenium salt **78** was confirmed in the solid state, finding a short P–B bond (1.989(2) Å, *r* = 1.04) and a trigonal planar B centre ($\Sigma_\alpha B$ = 360°). The N–B bond is short (1.384(2) Å, *r* = 0.89) again suggesting double bond character.

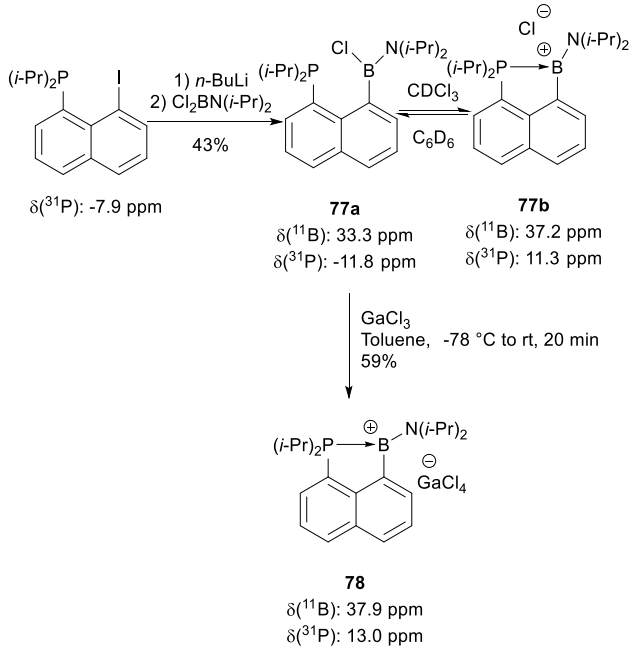

Scheme 22 Synthesis of the aminochloroborane **77a/b** and corresponding P-stabilised borenium salt **78**.

Given the lack of P→B interaction in **77a**, we postulated that the lone pair on P would be available for external reactivity. This was demonstrated by reacting **77a** with (tht)AuCl forming the corresponding phosphine gold(I) chloride complex **79** (Scheme 23). The ^{11}B NMR signal (35.4 ppm) remains almost identical to the parent compound suggesting the retention of a tricoordinate B centre. This bonding situation was confirmed in the solid state, with a trigonal planar B centre ($\Sigma_\alpha B$ = 358.9°). The P-Au-Cl skeleton is almost linear (173.1°). There is significant distortion in this system to accommodate the steric congestion imposed by all substituents as a P-C_{peri}-C_{peri}-B torsion angle of -43.9(1)° is observed. Interestingly, there is no spectroscopic or structural evidence of the presence of an Au→B interaction as may have been expected. This probably results from the reduced electrophilic character of the B centre due to π-donation from the amino substituent.

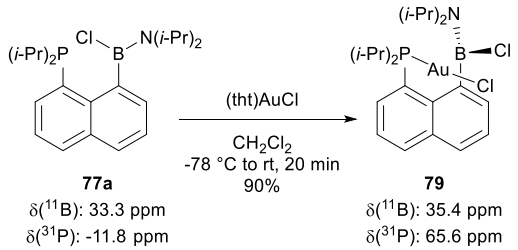

Scheme 23 Formation of phosphine gold(I) complex **79**.

Finally, **67** was also found to readily react with 3-hexyne through a carboboration reaction furnishing the phosphonium-stabilised vinyl borenium salt **80**, representing a rare example of 1,2-carboboration (Scheme 24).[43] The spectroscopic data of **67** and **80** are very similar due to the exchange of the aromatic substituent on B for a vinylic one. The upfield ^{11}B NMR signal (64.9 ppm) suggests a tricoordinate B centre. In a divergent reactivity pattern observed with the activation of H_2 and NH_3 bonds that yields neutral boranes, the 1,2-carboboration reaction transforms one borenium cation to another. However, in a similar fashion to the reaction with H_2, the B-Mes bond is cleaved. Here, it adds stereospecifically in *syn* fashion across the C≡C triple bond to form the vinyl borenium species **80**.

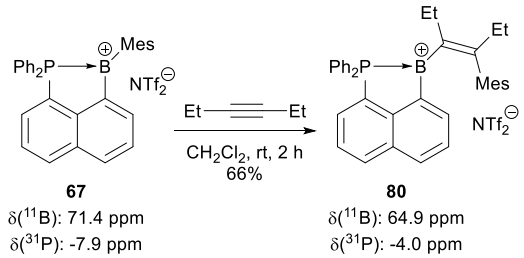

Scheme 24 1,2-Carboboration of 3-hexyne with **67**.

5.2. P-stabilised boryl radicals

Building on the body of work demonstrating the ability of naphthyl-enforced P→B interactions to stabilise reactive intermediates such as borenium cations, as described in the previous section, our group studied related boryl radicals. The ability to access such species was first assessed electrochemically by the reduction of the borenium cation **67**.[47] A quasi-reversible one-electron wave was observed at -0.48 V (vs. Fc^+/Fc), indicating much easier reduction than previously reported borenium/boryl couples whose potentials are significantly lower.

This encouraging result spurred the development of the chemical reduction of phosphine-bromoboranes **61** and **62** with 1.2 equivalents of 1% Na(Hg) amalgam in THF (Scheme 25).[47,48] X-band EPR analysis of the ensuing species **81** and **82** revealed complex but well resolved signals centred at g_{iso} = 2.0026. No change in the spectra was observed over days at room temperature, demonstrating the persistent character of these boryl radicals. Simulations successfully resolved the hyperfine structure taking into account couplings to ^{11}B (11.0 and 10.9 G for **81** and **82**, respectively) and ^{31}P nuclei (30.7 and 30.2 G for **81** and **82**, respectively) as well as two ^{1}H nuclei. The large $a(^{11}B)$ coupling indicates that spin density at B is unusually high. The values observed for **81** and **82** are in the upper range of previously reported persistent/isolable boryl radicals (7.3-13.2 G).[49–53] They are also higher than those of triphenyl- and trimesityl-boron anion radicals (7.8 and 9.9 G, respectively).[54–58] These coupling parameters were corroborated through theoretical calculations, which also allowed the attribution of the coupling to two ^{1}H nuclei on the naphthyl backbone (in

ortho and *para* positions with respect to B). This indicates that the unpaired electron is partly delocalized over the naphthyl framework. Accordingly, the SOMOs of **81** and **82** were calculated to be mainly localized on B (45.5% and 57.3%, respectively) with small contributions from P (8.9% and 9.3%, respectively) as well as the naphthyl backbone itself (*ipso*-C, *ortho*-C and *para*-C atoms with respect to B). The optimized structures of both boryl radicals show trigonal planar B centres (Σ_α = 359.6 and 360° for **81** and **82**, respectively) and short P–B bond lengths (1.908 and 1.913 Å, *r* = 1.008 and 1.002° for **81** and **82**, respectively). Intriguingly, the P→B interactions are shorter than in the corresponding borenium salts (1.997(6) and 2.006 Å, *r* = 1.05 for **65** and **67**, respectively). This is surprising given that the boryl radicals are less electrophilic than the borenium salts and would therefore be expected to display weaker P→B interactions. The shorter P–B bond length in **81** compared to **82** is also counterintuitive given the stronger P donation from (*i*-Pr)$_2$P. However, these observations can be rationalized by reduced negative 2p(B)→σ*(PC) hyperconjugation from (*i*-Pr)$_2$P compared to Ph$_2$P, this is supported by smaller contributions of P and C atoms in the Natural Localized Molecular Orbital (NLMO).

In the solid state, as determined unambiguously by X-ray crystallographic analyses, **81** and **82** dimerize to quinoid-type structures **[81]$_2$** and **[82]$_2$** (Scheme 25). The powders obtained upon crystallization are EPR silent confirming complete dimerization of the radicals. Dimerization occurs at the B centre of one unit and the *p*-C$_{Naphthyl}$ of another unit. Such Gomberg-type dimerization is quite rare for main group elements, as these radicals tend to dimerize through E–E bond formation (the central atom E is larger than C). The resulting C–B bond lengths (1.670(7) and 1.682(4) Å for **[81]$_2$** and **[82]$_2$**, respectively) are typical of single C–B bonds (sum of covalent radii B-C(sp^3) 1.60 Å, *r* = 1.04 and 1.05, respectively). The B centre directly involved in dimerization is tetracoordinate and pyramidalized (Σ_αB = 345 and 342.2°, THC = 49 and 52%, respectively), and the corresponding P–B bond length increases (2.115(6) and 2.131(3) Å, *r* = 1.11 and 1.12, respectively) due to steric hindrance. The other B centre remains trigonal planar (Σ_αB = 359.4 and 359.9°, respectively) and the associated P–B bond length is short (1.934(6) and 1.935(3) Å, *r* = 1.01, respectively). The C–B bond is shortened in this unit (1.463(6) and 1.458(4) Å) and is shorter than the sum of both covalent radii (B-C(sp^2) 1.57, *r* = 0.93, respectively) indicating double bond character.

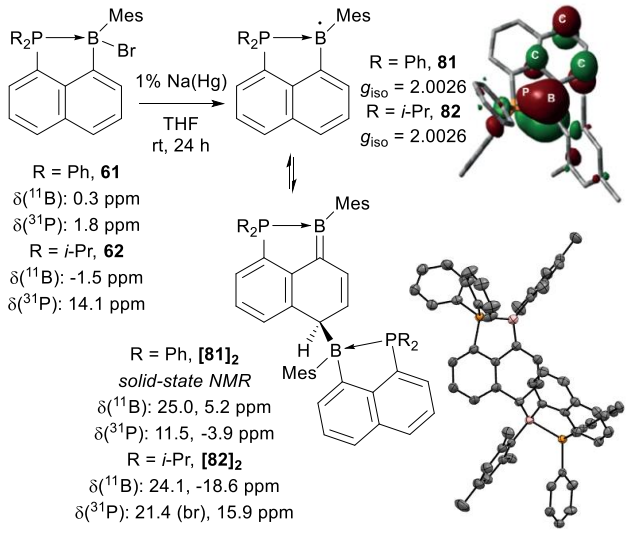

Scheme 25 Synthesis of the P-stabilised boryl radicals **81** and **82**, and their Gomberg-type equilibrium, SOMO of **81**; structure of the corresponding dimer [**81**]$_2$ with carbon in grey, phosphorus in orange, boron in pink and H atoms omitted for clarity.

Surprisingly, solutions of **81** and **82** are not NMR silent, the radical species are found to be in equilibrium with their corresponding dimeric quinoid-type structures **[81]$_2$** and **[82]$_2$** (Scheme 25). Due to the low solubility of **81**, the dimer **[81]$_2$** was fully characterized by solid state NMR, revealing two B (25.0 and 5.2 ppm) and P centres (11.5 and -3.9 ppm) in different environments. Solution NMR spectra of **82** revealed similar characteristics with two distinct signals for both the ^{11}B (24.1 and -18.6 ppm) and ^{31}P nuclei (21.4 and 15.9 ppm). The dimerization and equilibrium of both **81** and **82** with their respective dimers is analogous to that observed for the trityl radical ($Ph_3C^{\bullet}$).[59,60] The monomer/dimer equilibrium was analysed by VT EPR spectroscopy in toluene or THF/toluene (1:1) and the dimerization energy (ΔG) was estimated to be -15 and -12 kcal/mol for **81** and **82**, respectively. Substituting Ph for *i*-Pr on P increases spin density at B and favours the radical over its dimer. Additionally, calculations found that head-to-tail dimerization was preferred over B–B and *p*-$C_{Naphthyl}$–*p*-$C_{Naphthyl}$ coupling by >10 kcal/mol.

Aiming at exploring the effect of the substituent at B on the structure and stability of boryl radicals, novel phosphine-bromoboranes with highly sterically demanding aryl substituents at B, namely 2,4,6-triisopropylphenyl (Tip) and 2,6-dimesitylphenyl (Ter) were investigated (Scheme 26).[61] Derivatives **83** and **84** were synthesised by trapping (6-diphenylphosphinonaphth-5-yl)lithium with $TipBBr_2$ and $TerBBr_2$, respectively. Despite the steric crowding imposed by these bulky groups, high field ^{11}B (-0.1 and 0.7 ppm for **83** and **84**, respectively) and low field ^{31}P NMR signals (1.4 and 4.6 ppm, respectively) were maintained, indicative of tetracoordinate B centres and P→B interactions. This bonding situation was confirmed in the solid state for both **83** and **84** finding short P–B distances (2.024(2) and 2.080(7) Å, *r* = 1.06 and 1.09, respectively) and pyramidalized B centres (Σ_αB = 337.7 and 345.1°, THC = 49%, respectively). The naphthalene scaffold is found to respond to the steric bulk imposed by the Tip and Ter groups through significant distortions of both *peri* groups from the mean naphthalene plane (P-C_{peri}-C_{peri}-B torsion angles of 7.3(1)° and 20.8(4)° for **83** and **84**, respectively).

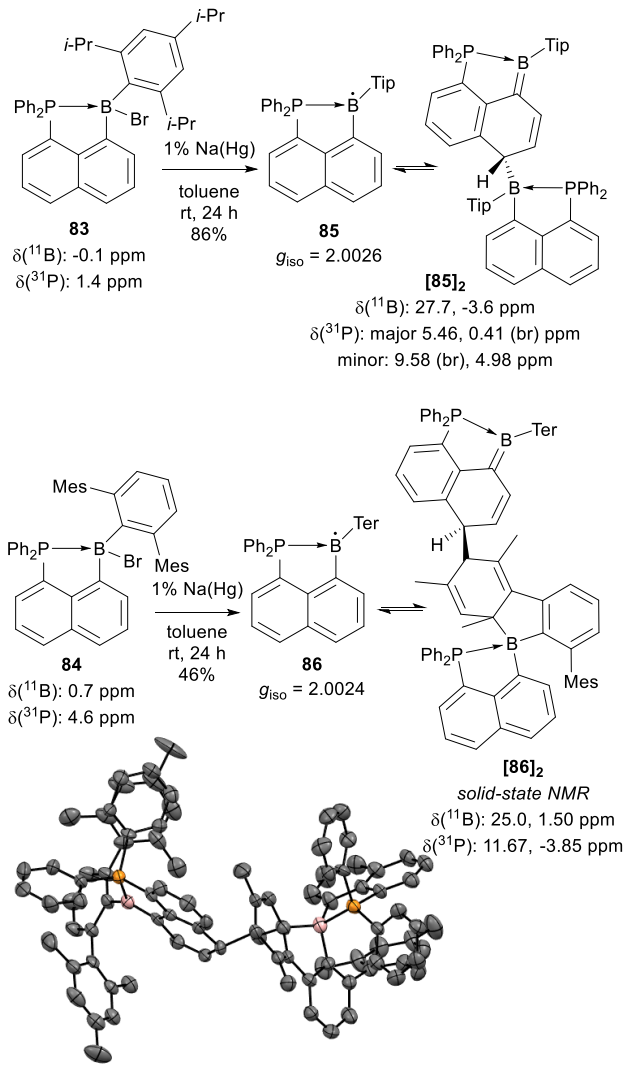

Scheme 26 Synthesis of the P-stabilised boryl radicals **85** and **86**, and their dimerization equilibrium; structure of **[86]$_2$** with carbon in grey, phosphorus in orange, boron in pink and H atoms omitted for clarity.

Reduction of **83** and **84** with 1.3 equivalent of a 1% Na(Hg) amalgam in toluene gave the corresponding boryl radicals **85** and **86** in moderate to high yields (Scheme 26).[47,48] The X-band EPR spectrum of **85** is very similar to those of **81** and **82**, with a well resolved signal centred at g_{iso} = 2.0026. The EPR spectrum of **86** also shows a complex and well resolved signal centred (g_{iso} = 2.0024) but its hyperfine structure somewhat differs from those of **81**, **82** and **85**. Larger couplings are found for **86** (11.5 and 31.4 G for ^{11}B and ^{31}P, respectively). The 11.5 G coupling to ^{11}B is the largest reported so far for a persistent boryl radical, indicating particularly high concentration of the spin density on B. No changes in the EPR spectra of **85** and **86** were observed over days at room temperature, demonstrating the stability and persistence of these P-stabilised boryl radicals.

Like **81** and **82**, solutions of **85** are not NMR silent, with spectra showing two sets of signals attributed to two diastereoisomers of the dimer **[85]$_2$** (Scheme 26). Similarly, dimerization of **[85]$_2$** occurs at the B centre of one unit and the *p*-$C_{Naphthyl}$ of another unit and presents similar structural parameters to **[81]$_2$** and **[82]$_2$**, as observed in the solid state. VT EPR spectroscopy was used to analyse the equilibrium between monomer and dimer finding ΔG = -9 kcal/mol. This is smaller than the dimerization energy observed for **81**, **82** and $Ph_3C^{\bullet}$ (-15, -12 and -11 kcal/mol) indicating that

the increased steric demand of the Tip moiety increases the thermodynamic stability of radical **85** but does not prevent its dimerization.

In the case of **86**, characterization of the residue by solid state NMR similarly shows two different environments for both B (25.0 and 1.5 ppm) and P centres (11.67 and -3.85 ppm). However, the solid-state structure reveals an original dimerization not previously observed with other P-stabilised boryl radicals. Dimerization occurs in this case between the naphthyl carbon *para* to B of one unit and the Ter substituent of another unit (Scheme 26). The B centre of the second unit couples with the *ortho* position of the Mes ring to form a quaternary C centre and a 1,4-cyclohexadienyl moiety while generating a boron-centred spiro motif. The newly formed C–C bond is long (1.61(1) Å, r = 1.06) and approaches the upper limit of known C(sp^3)-C(sp^3) bonds. The new B–C_{Mes} bond is long (1.66(1) Å, r = 1.04) with a tetracoordinate and pyramidalized B centre (Σ_αB = 342.1°, THC = 40%). The P–B bond in this unit is short at 2.05(1) Å (r = 1.07). The other B centre remains trigonal planar (Σ_αB = 359.9°) and the corresponding P–B bond is short (1.96(1) Å, r = 1.03). VT EPR experiments showed an equilibrium between monomer and dimer, but the kinetics were extremely slow, and the dimerization energy could not be estimated accurately. The Ter group imposes huge steric shielding to the B centre. This forces the boryl radical to react *via* remote positions although this dimerization pathway involves sites of low spin densities and disrupts the aromaticity of the naphthyl backbone and one Mes ring.

Given the similar dimerization energies of **82** and $Ph_3C^\bullet$ (-11 kcal/mol), we postulated that heterocoupling could occur. This was confirmed by mixing both species in benzene. Crystals of **87** spontaneously deposited, enabling X-ray diffraction analysis (Scheme 27). Similar to the homocoupling dimers described above, heterocoupling occurs between the central carbon atom of $Ph_3C^\bullet$ and *p*-$C_{Naphthyl}$ of **82**. The resulting C–C bond is very long (1.605(1) Å). The B centre remains trigonal planar (Σ_αB = 359.46°) and a short P–B bond is maintained (1.947(1) Å, r = 1.02). The B-C_{ipso} bond is short (1.466(2) Å, r = 0.93) signifying double bond character. To our knowledge, **87** is the first example of heterocoupling of $Ph_3C^\bullet$ with a persistent radical of a p-block element. Calculations reproduced the coupling of the boryl and trityl radicals. Another minimum was located on the potential-energy surface for the B–C_{Trityl} coupling product. It displays a long B–C_{Trityl} bond (1.760 Å, r = 1.10) and sits 6.2 kcal/mol higher in energy compared to the *p*-$C_{Naphtyl}$-C_{Trityl} coupling product.

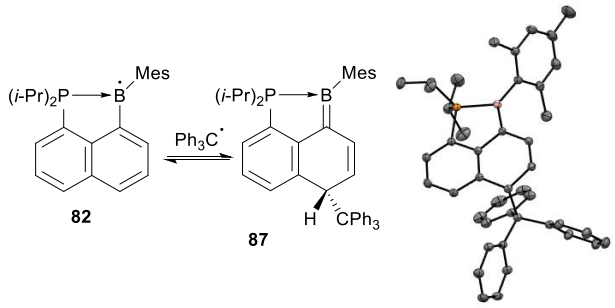

Scheme 27 Heterocoupling of **82** with $Ph_3C^\bullet$; structure of **87** with carbon in grey, phosphorus in orange, boron in pink and H atoms omitted for clarity.

Prompted by the heterocoupling observed with $Ph_3C^\bullet$, we then investigated the trapping of the phosphine-boryl radicals **81** and **82** with the stable 2,2,6,6-tetramethylpiperidine-1-oxyl (TEMPO) radical (Scheme 28). Reactions occurred rapidly at room temperature to give 1:1 [R_2P(naph)BMes/TEMPO] adducts **88** and **89** in high yields. The observed low field ^{11}B NMR signals

(40.7 and 43.0 ppm for **88** and **89**, respectively) are indicative of tricoordinate B centres while the high field ^{31}P NMR signals (-9.52 and -5.3 ppm, **88** and **89**, respectively) support the lack of intramolecular P→B interactions. These spectroscopic data suggest that these products adopt open structures. The B Lewis acidity is lower due to strong O→B π-donation of the TEMPO substituent, similar to that encountered in the previously described phosphine-aminoboranes **73**, **74** and **77a**. These bonding situations were unambiguously confirmed in the solid state, finding trigonal planar B centres (Σ_αB = 358.8 and 357.9° for **88** and **89**, respectively). The P–B distances are long (2.922(2) and 2.901(2) Å, *r* = 1.53 and 1.52), while the B–O bond are short (1.376(3) and 1.385(2) Å, *r* = 0.92 for **88** and **89**, respectively), suggesting double bond character. The naphthyl scaffold displays flexibility in allowing significant distortions of the *peri* groups from the mean naphthalene plane P-C_{peri}-C_{peri}-B torsion angles of 30.3 and 12.6° for **88** and **89**, respectively) to avoid steric repulsions from the bulky groups on P and B. In this case, heterocoupling selectively occurs at B where most of the spin density is concentrated. No coupling to the *p*-$C_{Naphthyl}$ site was observed.

The phosphine-boryl radicals were also found to be reactive in radical chlorine transfer reactions, with trityl chloride (Ph_3CCl), to give the corresponding phosphine-chloroboranes (**90** and **91**) in good yields (Scheme 28). The high field ^{11}B NMR signals (5.3 and 1.5 ppm for **90** and **91**, respectively) are diagnostic of tetracoordinate B centres. The ^{31}P NMR signals (2.1 and 15.4 ppm, respectively) are very similar to those of the related phosphine-bromoboranes **61** and **62** (1.8 and 14.1 ppm, respectively). The solid-state structure of **90** was analysed by X-ray diffraction, showing a short P–B bond (2.063(2) Å, *r* = 1.08) and a pyramidal geometry at B (Σ_αB = 339.8°, THC = 56%). The formation of **90** and **91** represents rare examples of halogen transfer to a B centred radical and highlights the spin density concentration at the B centres. Despite increased steric crowding at B in **85**, radical reactivity is maintained at the B centre, as demonstrated by its heterocoupling with TEMPO and radical halogen transfer reactions with Ph_3CCl to give the corresponding 1:1 adduct (**92**) and phosphine-chloroborane (**93**), respectively (Scheme 28).

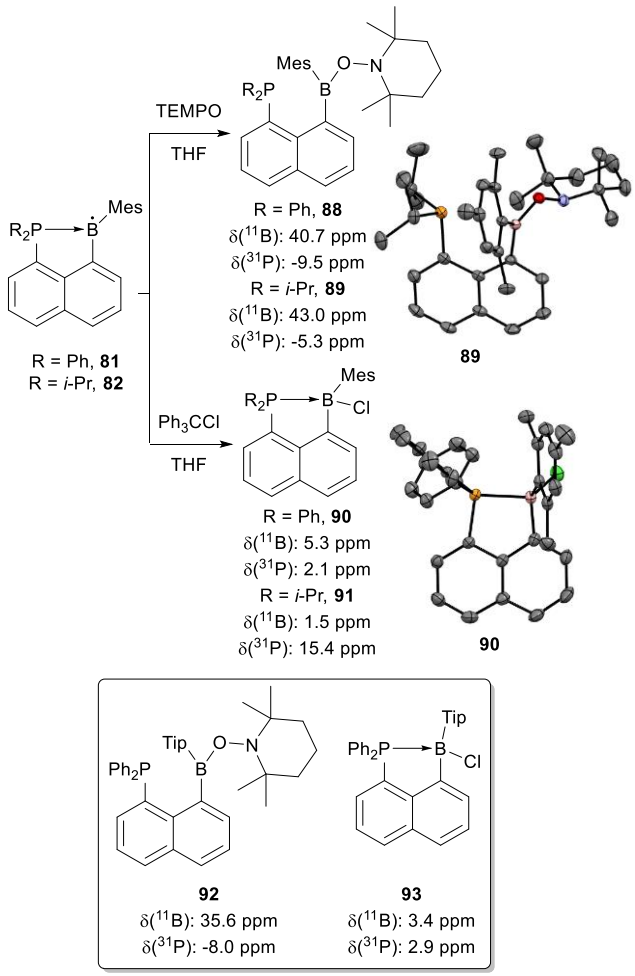

Scheme 28 Reactivity of the P-stabilised boryl radicals **81**, **82** and **85** with TEMPO and Ph_3CCl; structures of **89** and **90** with carbon in grey, phosphorus in orange, nitrogen in blue, oxygen in red, boron in pink, chlorine in green and H atoms omitted for clarity.

5.3. N/P-stabilised borylenes

The synthesis, characterisation and reactivity of borylenes is an emerging field of research with increasing interest given to metal-free Lewis base stabilised borylenes (Chart 9).[49,62–64] While P-based exogenous Lewis bases have been used to stabilise and characterize borylene species,[65,66] to date, there are no reports of isolated borylene derivatives incorporating the (ace)naphthalene with amino or phosphino groups at the *peri* position.

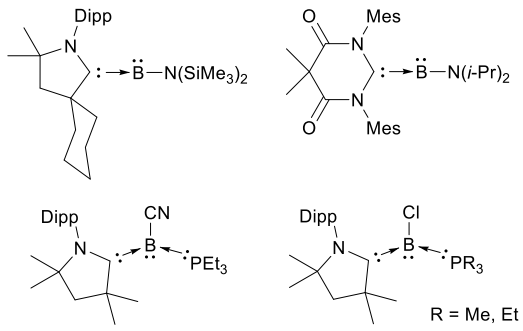

Chart 9 Selected examples of borylenes stabilised by one (top row) or two (bottom row) Lewis base(s).

However, these systems have gained interest for their synthetic challenge, their unusual electronic structure and their potential reactivity. Lu, Wu *et al*. reported in 2019 a systematic study of a series of LB→BR borylenes, analysing the effect the Lewis base and substituent have on the electronic structure and geometry of these intriguing species.[67] In particular, they optimized the structures and calculated singlet-triplet gap energies (ΔE_{ST}) of 1-dimethylamino- (**94**) and 1-dimethylphosphino-naphthyl (**95**) borylenes (Chart 10). The N-B derivative **94** is calculated to have a very small difference between its singlet and triplet state energies (ΔE_{ST} = 1 kJ/mol) suggesting that both the singlet and triplet states may be accessible. The N–B bond in **94** is shorter in the triplet state (1.62 Å, *r* = 1.09) than in the singlet state (1.78, *r* = 1.15). This is accompanied by a shortening of the C–B bond (1.49 and 1.58 Å, *r* = 0.95 and 1.00, for the triplet and singlet states, respectively), the length of which is suggestive of some double bond character. The N-B-C bond angle also widens in the triplet vs. singlet state (106.5 vs. 95.1°). Both configurations display high coplanarity of the entire molecular structure, as apparent from the null N-C_{peri}-C_{peri}-B torsion angle. Contrary to **94**, the triplet state is highly favored as ground state for the P-B derivative **95** (ΔE_{ST} = -37 kJ/mol). Similar bond contractions are observed from the singlet to the triplet state: the P–B bond shortens from 2.00 to 1.89 Å (*r* = 1.05 to 0.99) while the C–B bond length decreases from 1.59 to 1.52 Å (*r* = 1.01 to 0.97). The P-B-C angle is also significantly more open in the triplet state (104.6°) than in the singlet state (94.6°). The optimised structure of **95** reveals significant distortions of both *peri* groups from the mean naphthalene plane (P-C_{peri}-C_{peri}-B torsion of -10.1°) as well as slight torsion of the naphthalene scaffold itself. In contrast, the structure of the triplet state displays high coplanarity, with no distortions of either *peri* group or the naphthalene backbone. While known examples of mono-Lewis base stabilised borylenes display near linear geometry (174.8–179.5°), **94** and **95** are anomalies with highly bent structures (the computed E^{15}-B-C bond angles are all below 106.5°). These geometrical constraints certainly play a role in the fact that the singlet state is not energetically favored for borylenes **94** and **95**.

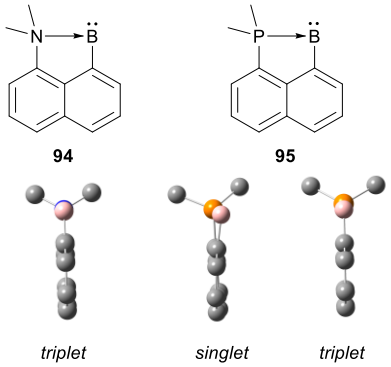

	ΔE_{ST} (kJ/mol)	E^{15}-B (Å)		C_{peri}-B (Å)		E^{15}-B-C_{peri} (°)		E^{15}-C_{peri}-C_{peri}-B Torsion (°)	
		Singlet	Triplet	Singlet	Triplet	Singlet	Triplet	Singlet	Triplet
94	-1	1.78	1.62	1.58	1.49	95.1	106.5	0	0
95	-37	2.00	1.89	1.59	1.52	94.6	104.6	-10.1	0

Chart 10 N- and P-stabilised borylenes **94** and **95** with key computed structural parameters; optimised structures (side views) with carbon in grey, nitrogen in blue, phosphorus in orange, boron in pink and H atoms omitted for clarity.

6. Heavier pnictogen E^{15}-B naphthalene derivatives

As discussed above, numerous groups have investigated the ability of the naphthalene scaffold to enforce short contacts between N or P and B at the *peri* positions. The use of heavier group 15

congeners is much more limited, with a single contribution. Gabbaï *et al*. reported in 2011 the synthesis and structure of E^{15}-B naphthyl derivatives with antimony (**96**) and bismuth (**97**) (Scheme 29).[68] Their synthetic strategy leverages the ring strain of the dimesityl-1,8-naphthalenediylborate to react with either Ph_2SbCl or Ph_2BiCl. Ring opening provides the corresponding E^{15}-B derivative in moderate to good yields. Steric crowding imposed by the substituents on both E^{15} and B results in unsymmetrical Mes groups, as evidenced by six distinct Me signals in the ^{1}H NMR spectra. However, ^{11}B NMR signals (66 and 68 ppm for **96** and **97**, respectively) are consistent with tricoordinate B centres, suggesting the absence of strong $E^{15}\rightarrow$B interactions. This bonding situation was confirmed in the solid state, finding E^{15}–B distances (3.216 and 3.330 Å for **96** and **97**, respectively) which are longer than the sum of their respective covalent radii (2.23 and 2.32 Å, for Sb-B and Bi-B, respectively; *r* = 1.44) and trigonal planar B centres (Σ_αB = 358.7 and 359.2° for **96** and **97**, respectively). The naphthyl backbone accomodates the steric demand imposed by the substituents on E and B by deviating *peri* bond angles above the ideal 120° (122.5(4) to 130.6(5)°) as well as distorting both *peri* groups from the mean naphthalene plane (0.337 to 0.492 Å). As expected from the larger size of Sb and Bi, the E^{15}–$C_{Naphthyl}$ bonds (2.157(6) and 2.268(6) Å for **96** and **97**, respectively) are significantly longer than the B–$C_{Naphthyl}$ bonds (1.589(8) and 1.575(9)Å for **96** and **97**, respectively), which places E^{15} above B in the plane of naphthalene scaffold and prevents strong $E^{15}\rightarrow$B interactions (Scheme 29).

The DFT-optimised structures nicely reproduced those determined crystallographically, with the exception of slightly longer E^{15}–B distances (3.410 and 3.448 Å for **96** and **97**, respectively). Interestingly, NBO analyses indicate the presence of weak $E^{15}\rightarrow$B interactions (deletion calculations lead to energy increases of 8.6 kcal/mol for **96** and 6.3 kcal/mol for **97**). The rigid naphthyl scaffold plays a major role in these weak $E^{15}\rightarrow$B bonding interactions. Indeed, attempts to optimize Lewis pair structures for the corresponding intermolecular adducts $Ph_3E^{15}\rightarrow BPh_3$ systematically led to complete dissociation.

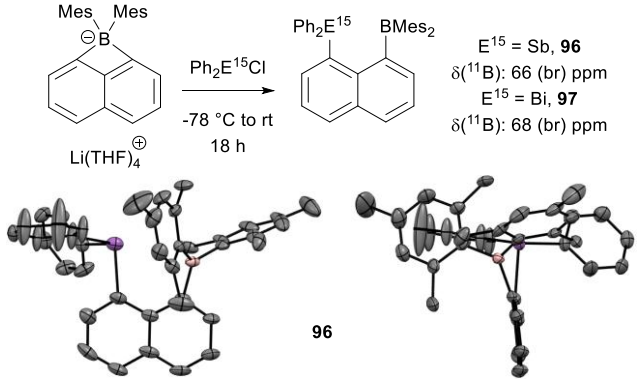

Scheme 29 Synthesis of the Sb- and Bi-B compounds **96** and **97**; structures of **96** (front and side views) with carbon in grey, antimony in purple, boron in pink and H atoms omitted for clarity.

7. Biphenylene, (Thio)Xanthene and Dibenzofuran-bridged P-B derivatives

Biphenylene, (thio)xanthene and dibenzofuran scaffolds can be viewed as expanded naphthalene systems incorporating cyclobutadiene, (thio)pyran or furan moieties. P-B derivatives featuring these spacers have been studied and shown to display properties complementary to those of (ace)naphthyl-bridged compounds. As discussed, hereafter, the long distances imposed between P and B (Chart 11) impart unusual coordination modes and favors reversible interaction with small molecules such as H_2 and N_2O.

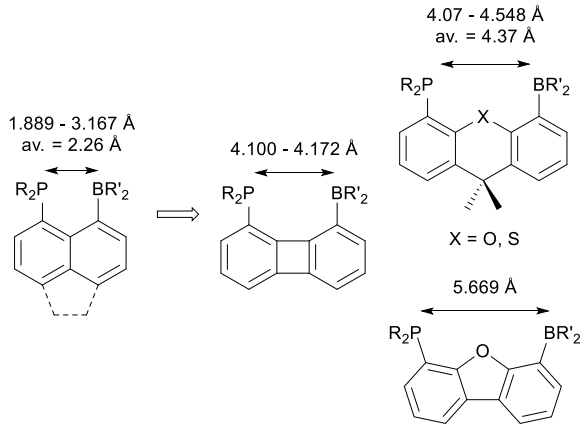

Chart 11 Comparison of ranges and average P-B distances in crystallographically characterised (ace)naphthalene, dibenzofuran, biphenylene, and (thio)xanthene compounds.

The first such P-B derivative featuring a rigid expanded spacer, **98**, was reported by Emslie *et al.* in 2006 (Chart 12).[69] It was obtained in 66% overall yield by stepwise lithiation phosphination and borylation. Reversible coordination of acetonitrile to boron was used to isolate **98** in pure form. Its extreme solubility even in apolar solvents prevents the growth of crystals and X-ray diffraction analysis, but spectroscopic data clearly indicate that no P→B interaction occurs, and the structure remains open. The reactivity of this derivative towards small molecules has not been reported, but its coordination properties have been extensively investigated. The ambiphilic nature of **98** results in original complexes featuring unusual coordination modes (see Chart 12 for representative examples). Due to the open nature of **98**, the P moiety is available to bind metals, while the Lewis acidic B functionality is ready to interact with co-ligands in the second coordination sphere (such as in the Pd(dba) complex **99**).[69] The □-delocalized BPh_2 fragment is also prone to engage in multicenter η^2-BC_{ipso} and η^3-$BC_{ipso}C_{ortho}$ coordination,[70] as observed with Rh (**100**),[71] Pd (**101**) and Ni (**102**)[72]. Additionally, the P-B ligand **98** allowed the observation of bridging M–X–B interactions with Pd (**103**), Pt (**104**)[72,73] and Rh (**105**-**107**)[74]. Of interest, reaction of **98** with [$PtMe_2$(COD)] enables the detection and characterisation of the zwitterionic complex **108**, en route to the rearranged complex **109** (with Ph groups now at Pt and Me groups now at B). Here, the Lewis acid moiety abstracts the co-ligand from the metal, opening the way for methyl/aryl exchange between the platinum and boron.[75]

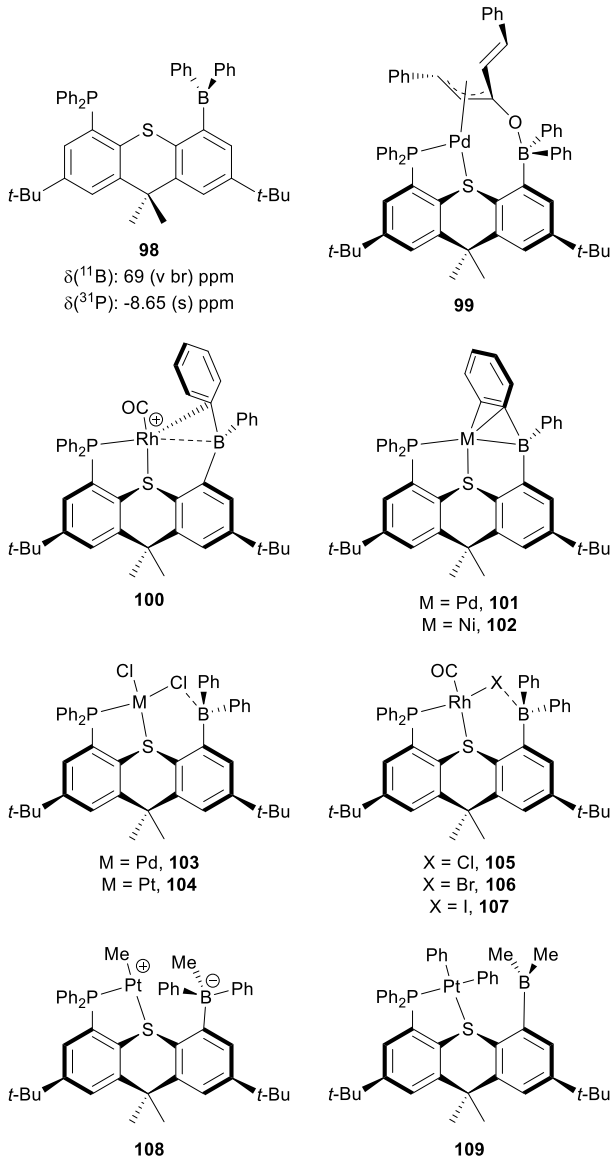

Chart 12 Thioxanthene-bridged P-B ligand **98** and representative complexes thereof.

Looking towards the development of FLPs for potential applications as chemical sensors and catalysis, several groups have investigated novel single component phosphine-boranes displaying reversibility in the activation of small molecules. They postulate that a geometrically constrained FLP with a P-B separation in the 4.2-4.8 Å range may allow for the reversible activation of H_2.[76,77] This supposition is built on the premise that once H_2 is activated, the lack of conformational flexibility of the backbone and the confinement of the resultant hydridic/protic H atoms in close proximity preorganises the system for H_2 release (Chart 13). In such a situation, the activation energies of both the forward and reverse processes were expected to be lowered.

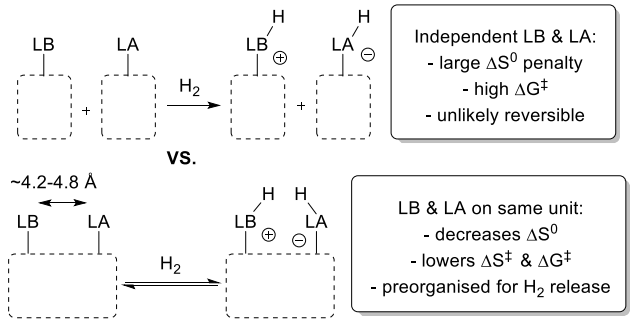

Chart 13 Concept and strategy of preorganised FLPs for the reversible activation of H_2.

With this goal in mind, they turned to dibenzofuran and dimethylxanthene backbones, and prepared new P-B derivatives by stepwise lithiation phosphination and borylation (**110** and **111**-**114**, Scheme 30).[76,77] All derivatives adopt FLP-type structures without P→B interactions. The ^{11}B NMR chemical shifts (58.2-69.5 ppm) are diagnostic of tricoordinate B centres, while the ^{31}P NMR shifts are indicative of free phosphines. This is further evidenced in C_6F_5-containing derivatives **110**-**114** by large differences (>10 ppm) in ^{19}F NMR chemical shifts between the *m*- and *p*-F signals (Scheme 30).[27] The lack of P→B interactions was confirmed in the solid-state for all derivatives, finding trigonal planar B centres (Σ_αB = 359.6-360°) and long P–B distances (4.070(2)-5.669(1) Å, r > 2).

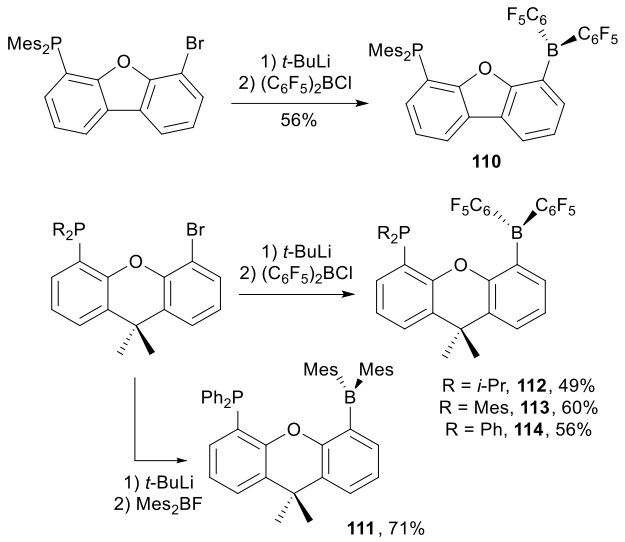

(ppm)	**110**	**111**	**112**	**113**	**114**
$\delta(^{11}B)$	59.2	69.5	65.0	64.4	58.2
$\delta(^{31}P)$	-38.1	-19.6	-9.91	-38.0	-15.5
$\Delta\delta(^{19}F_{m\text{-}p})$	13.1	-	13.4	20.1	15

Scheme 30 Synthesis and key NMR data of dibenzofuran **110** and xanthene derivatives **111-114**.

The propensity of these derivatives to activate H_2 was then investigated. Both **110** and **111** were found to be unreactive towards H_2. This was rationalised by the large P–B separation in **110** and by the weak Lewis acidity/basicity of **111**. Increasing both the Lewis acidity of B and the Lewis basicity of P, such as in **112**, allows for the activation of H_2 (Scheme 31). The resulting phosphonium borate **115** was characterised in the solid-state, confirming the activation of H_2. Upon H_2 activation, the B centre strongly pyramidalizes (Σ_αB = 335.3(2)°, THC = 79%), the P–B distance shortens (from 4.487(3) Å, r = 2.35 in the parent FLP **112**, to 4.104(3) Å, r = 2.15 in **115**), while the H–H separation is 2.07(5) Å. The phosphonium borate **115** seems predisposed for H_2 release, due to the rigid structure that confines the hydridic and protic components to the central cavity, but no detectable H_2 release could be observed from **115** even upon heating to 80 °C. The lack of reversibility is attributed to the σ-donating *i*-Pr substituents at P, which make the reverse reaction energetically unfeasible.

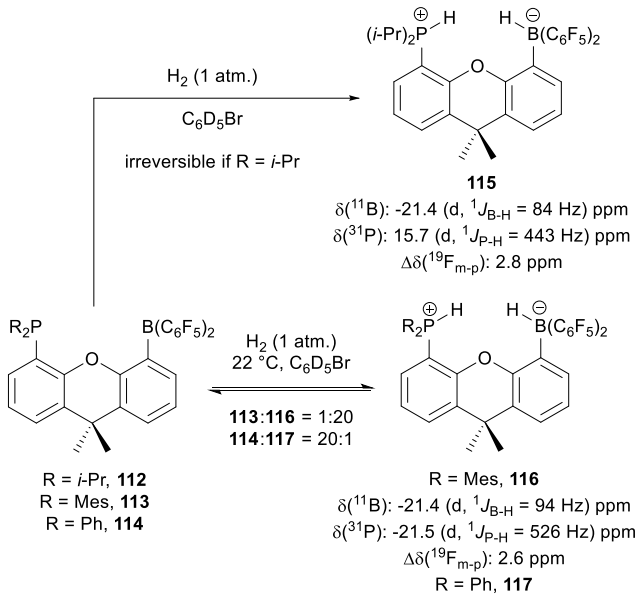

Scheme 31 (Reversible) activation of H_2 by **112**-**114**.

Upon decreasing the Lewis basicity with Mes groups at P, activation of H_2 is maintained but the process is now reversible. Compound **113** enables uptake and release of H_2 (Scheme 31). The structure of the ensuing phosphonium borate **116** was confirmed spectroscopically and crystallographically, displaying similar characteristics to **115**. D_5-bromobenzene solutions of **116** show an equilibrium between free FLP **113** and **116** (1:20, at 22 °C, respectively). Varying the temperature allowed the determination of the thermodynamic parameters ΔH^0 = 38 kJ/mol and ΔS^0 = 102 J/mol/K. This can be compared to the *p*-(Mes_2PH)-C_6F_4-[$B(C_6F_5)_2H$] system described by Stephan *et al*. in which H_2 release occurs at temperatures greater than 100 °C, with the thermodynamic parameters ΔH^0 = 90 kJ/mol and ΔS^0 = 96 J/mol/K.[78] The lower magnitude of the enthalpic term for **113**, due to the lower Lewis acidity/basicity of B and P, respectively, facilitates the release of H_2 at much lower temperatures. The free energies for H_2 release (ΔG_{H2}) were calculated for the phosphonium borates deriving from **110** (-6.40 kcal/mol), **112** (-0.97 kcal/mol) and **113** (-1.85 kcal/mol).[79] These data match well the experimental observations and highlight the effects of the backbone (**110**) and substituents on P (**112** vs. **113**). Further reduction of the Lewis basicity of P by incorporating Ph groups (**114**) makes the uptake of H_2 less favored thermodynamically (Scheme 31). Solutions of **114** in d_5-bromobenzene under 4 atm. of H_2 show only 5% conversion to the phosphonium borate **117** at 22 °C. Thermodynamic parameters could be determined, finding ΔH^0 = 34 kJ/mol and ΔS^0 = 138 J/mol/K.

The reversibility of H_2 activation motivated the authors to investigate the xanthene-derived P-B compounds as catalysts for dehydrogenation reactions. In particular, **114** for which H_2 release is facile, was shown to be capable of dehydrogenating dimethylamine-, methylamine- and amine-borane under mild conditions (1 mol%, 55 °C). This stands as a rare example of a metal-free catalyst for this process (Scheme 32).[77] Detailed experimental mechanistic investigations were undertaken, involving stoichiometric reactions as well as the independent syntheses of off-cycle products and reaction intermediates. These studies allowed the authors to confirm that oligomerisation is initiated by B–H activation, forming first the phosphonio-borate **118**. This is followed by stepwise end-growth B–N coupling (between a terminal N–H bond of the bound fragment and a B–H bond of the incoming monomer), releasing H_2 and giving intermediate **119**. After each monomer coupling, the resulting P-bound amino-borane chain is engaged in NH···$HB(C_6F_5)_2$ hydrogen bonding (in **119**,

the H–H distance is 1.85 Å). Coupling a third monomer results in the formation of the cyclic borazane, which finally affords the borazine upon dehydrogenation (Scheme 32).

The phosphine-borane **114** was also found competent in B–H bond activation, albeit with a different mode of reactivity than that presented above. Reactions of **114** with pinacolborane (HBpin) and catecholborane (HBCat) induces boryl exchange at the xanthene backbone *via* B–C/B–H σ-bond metathesis, and the released Piers' borane $HB(C_6F_5)_2$ is trapped by the P centre as a classic Lewis adduct (Scheme 33).[80] The resulting derivatives **120** and **121** have been spectroscopically and crystallopgraphically characterized. They display two sets of ^{11}B NMR signals in the typical range for tri- and tetracoordinate B centres. Interestingly, compounds **120** and **121** were independently synthetised from the analogous xanthene-bridged FLPs incorporating Bpin and Bcat moieties, **122** and **123**, respectively (Scheme 33). Similar to the $BMes_2$ and $B(C_6F_5)_2$ derivatives **111**-**114**, the scaffold prevents the formation of P→B interactions in **122** and **123**. The B centres remain tricoordinate as apparent from ^{11}B NMR spectroscopy (31.0 and 32.0 ppm, respectively), and X-ray diffraction analyses: the B centres adopt trigonal planar environments ($\Sigma_\alpha B$ = 360° and 359.9(2)°, respectively) and the P–B distances are long (4.548(2) and 4.377(2) Å, *r* = 2.38 and 2.29, respectively).

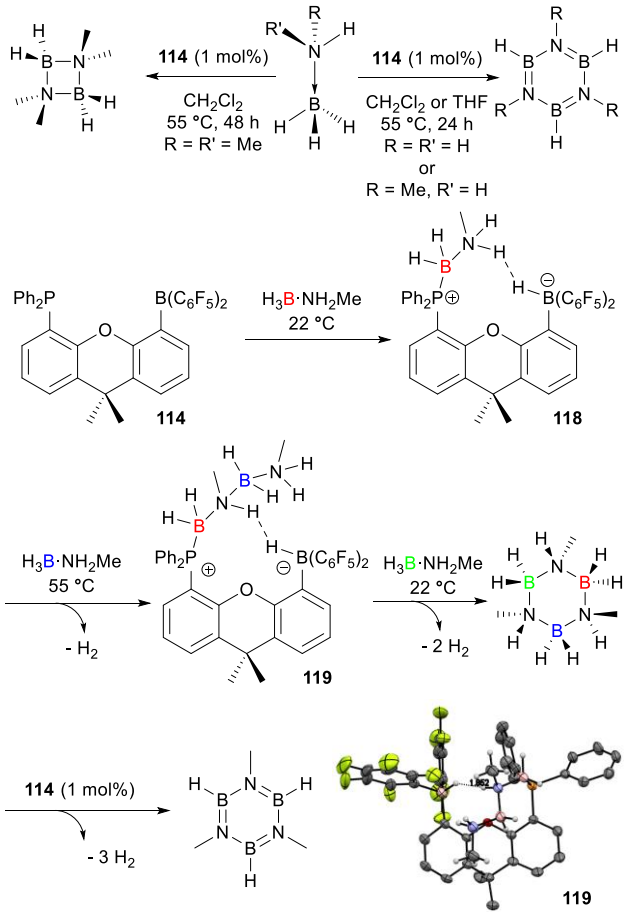

Scheme 32 Catalytic dehydrogenation of amino-boranes by **114** and associated mechanism; X-ray structure of intermediate **119** with carbon in grey, nitrogen in blue, boron in pink, oxygen in red, fluorine in green, phosphorus in orange, and H atoms of backbone omitted for clarity.

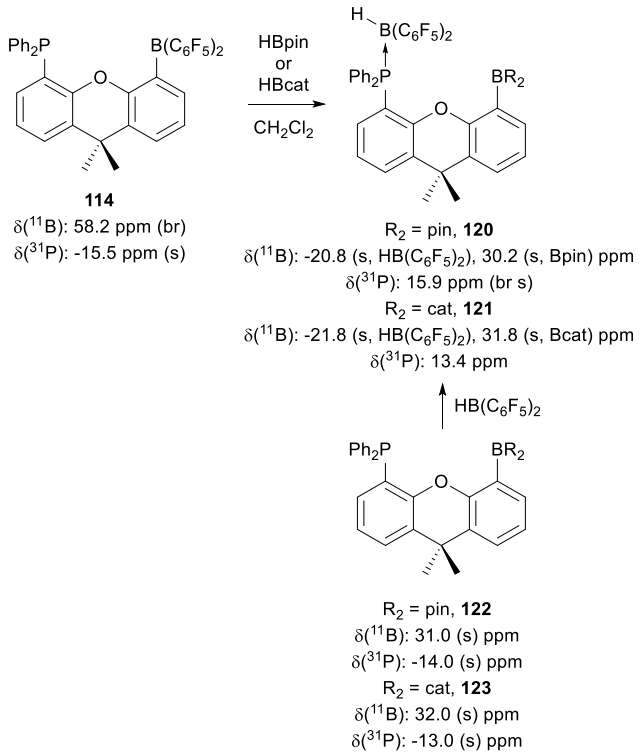

Scheme 33 Activation of B–H bonds and boryl exchange with **114**.

In line with the reactivity of xanthene-bridged P-B derivatives described thus far, Vasko, Kamer, Aldridge *et al.* reported the ability of **113** and **114** to activate C(sp)–H bonds.[80] Derivatives **113** and **114** react with phenylacetylene (PhCCH) to provide the corresponding phosphonium alkynylborates **124** and **125**, respectively (Scheme 34). Interestingly, the C(sp)–H activation is reversible with the PPh_2 compound **114** (solutions of **125** show signals related to **114** and free PhCCH), but not with **113** featuring a more basic $PMes_2$ moiety. Solid-state analysis of **124** confirms the activation mode of the alkyne, finding a P–H phosphonium group and a nearly linear B–CCPh borate fragment (171.7°). While solutions of **124** are stable, **125** undergoes further transformation over the course of several hours to give the peculiar phosphonium borate **126** incorporating two additional molecules of phenylacetylene, as elucidated by X-ray crystallography (Scheme 34). The formation of **126** is inherently linked to the reversibility of the reaction of **114** with PhCCH. It requires the presence of free alkyne in solution and most likely involves 1,2-addition of the P-B derivative to the C≡C bond. The feasibility of such a transformation was established using a more electron-rich alkyne, 4-methoxyphenylacetylene (4-$MeOC_6H_4CCH$). This affords the phosphonium borate **127** (79% yield) as the result of regioselective *trans* 1,2-addition of the P and B center to the alkyne. The structure of **127** was unambiguously authenticated thanks to multi-nuclear NMR spectroscopy and X-ray diffraction analyses.

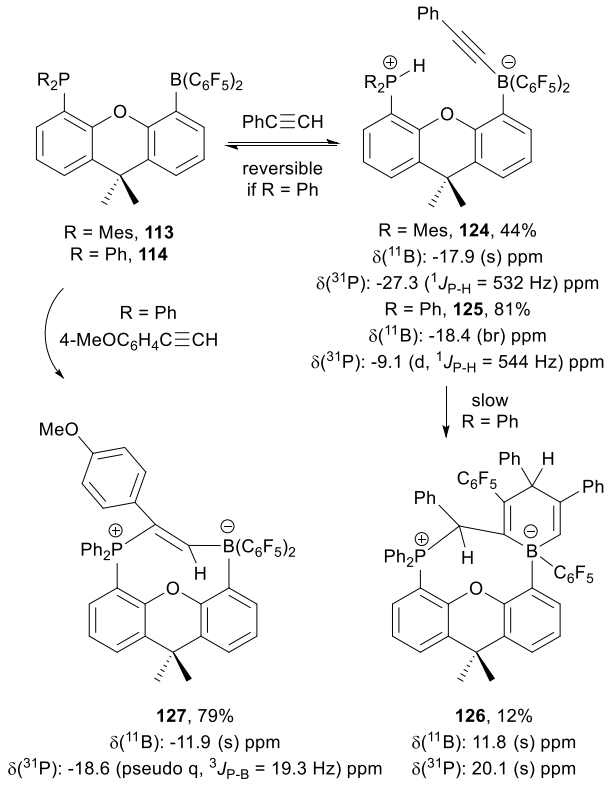

Scheme 34 Reaction of **113** and **114** with terminal alkynes: C(sp)–H bond activation vs. 1,2-addition.

Given the capacity of **114** to activate both B–H bonds and alkynes, it was tested for the catalytic hydroboration of alkynes with HBpin (Scheme 35).[80] The reaction is complete within a few hours at room temperature with 10 mol% catalytic loading. Given the boryl exchange reaction observed between **114** and HBpin, the active species is believed to be in fact $HB(C_6F_5)_2$,[81,82] and the slower catalytic performance with PhCCH compared to PhCCMe is attributed to the sequestering of **114** as unreactive **125** and **126**.

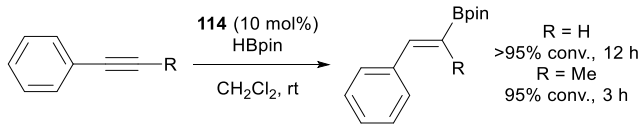

Scheme 35 Catalytic hydroboration of alkynes with **114**.

The interaction of **113** and **114** with O–H bonds was also investigated (Scheme 36).[83] Initially, **114** was found to only form simple Lewis adducts with H_2O, MeOH and *i*-PrOH, as established spectroscopically and crystallographically. The acidity of the O–H bond was postulated to play a major role in its activation, and indeed upon reacting the more acidic 4-*tert*-butylphenol (4-*t*-BuC_6H_4OH) with **113** and **114**, the resulting phosphonium borates **128** and **129** were obtained (Scheme 36). Spectroscopic data evidence the formation of phosphonium centres in both **128** and **129**, and these structures were unambiguously confirmed by X-ray diffraction analyses. Intriguingly, when crystals of **129** were dissolved in d_6-benzene, NMR spectra consistent with the simple Lewis adduct **130**, not **129**, were obtained (Scheme 36). The reversibility of this process was further confirmed through VT-NMR experiments. The phosphonium borate **129** structure is found at low temperatures (-16 °C), while at higher temperatures, the Lewis adduct **130** predominates. Here, the reversibility of the O–H activation process with **129** contrasts with the stability of **128**. This is again

attributed to the stronger basicity of the $PMes_2$ moiety compared to PPh_2. These findings were confirmed by DFT calculations: the Lewis adduct **130** was found to be 8.3 kJ/mol more stable than **129** at 25 °C, and a transition state was located at 9.2 kJ/mol confirming the lability of the O–H bond in **129**. On the other hand, **128** was found to be 34.6 kJ/mol more stable than its corresponding Lewis adduct, highlighting the irreversibility of the process.

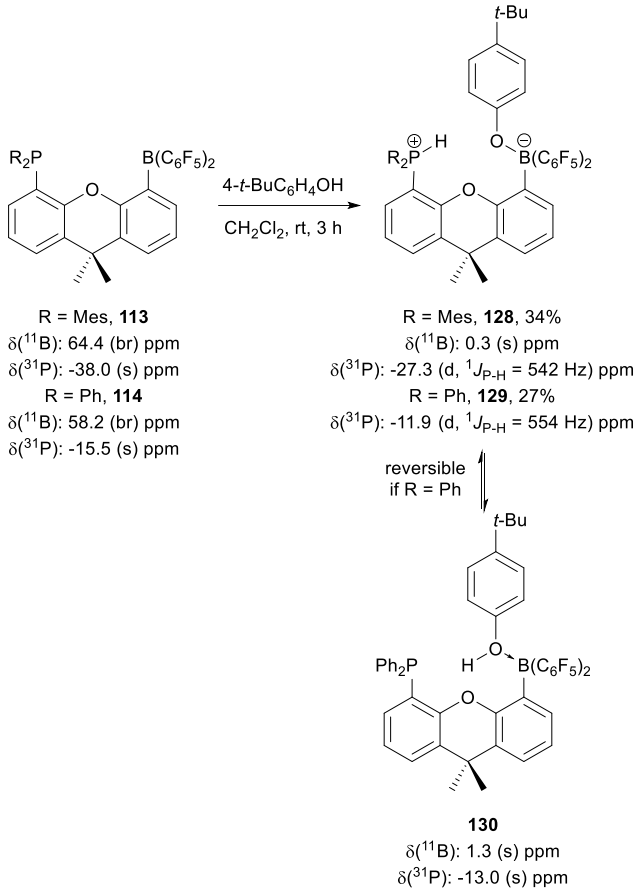

Scheme 36 Reactions of **113** and **114** with 4-*tert*-butylphenol.

Finally, Aldridge *et al.* also showed that the FLP cavity in **113** is appropriately sized for the capture and activation of nitrous oxide (N_2O) (Scheme 37).[76] Reacting a CH_2Cl_2 solution of **113** under a 1 atm. of N_2O results in the formation of the 1:1 adduct **131** (75% isolated yield). The upfield ^{11}B NMR signal (4.3 ppm) is indicative of a tetracoordinate B centre, while the downfield ^{31}P NMR signal (46.8 ppm) is consistent with quaternisation of the P centre. The uptake of N_2O was confirmed in the solid-state, revealing a PNNOB unit of W configuration bound in the cavity. Here, the dimethylxanthene scaffold displays some flexibility and responds to the incorporation of the N_2O unit by expanding the P–B separation by ~0.3 Å compared to **113**. This distortion is presumed to favour the release of N_2O at elevated temperatures. Upon heating solutions of **131** at 50 °C, the P-B derivative **113** was recovered quantitatively with no competing formation of phosphine oxide derivatives. This was the first example of reversible N_2O fixation.

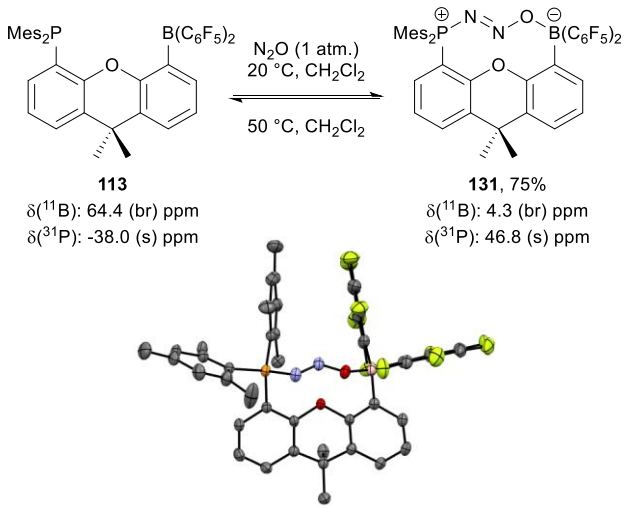

Scheme 37 Reversible fixation of N_2O by **113**; X-ray structure of **131** with carbon in grey, nitrogen in blue, boron in pink, oxygen in red, fluorine in green, phosphorous in orange, and H atoms omitted for clarity.

In 2018, the groups of Beckmann and Erker independently developed FLP derivatives based on the biphenylene scaffold.[84–86] They both relied on the premise that single component FLPs could offer potential advantages over two component FLP systems. In particular, Beckmann *et al.* surmised that a rigid scaffold maintaining donor and acceptor moieties at 3-5 Å may be necessary for high catalytic activity.[87–90] In this context, they prepared the new P-B derivative **133** by stepwise lithiation, phosphination and borylation (Scheme 38).[84] While no ^{11}B NMR signal could be observed for **133**, the ^{31}P NMR signal at -19.5 ppm is highly indicative of the lack of P→B interaction. This bonding situation was confirmed in the solid state by X-ray diffraction analysis, finding two independent molecules in the unit cell with trigonal planar B centres ($\sum_\alpha$B = 359.3(1) and 359.5(1)°) and long P–B distances (4.100(2) and 4.172(2) Å, $r > 2$) confirming the FLP nature of **133**. Despite the prerequisite P–B distance, no reactivity with H_2 or CO_2 could be observed. The authors tentatively attribute the lack of reactivity to the low Lewis acidity of B. They attempted to incorporate C_6F_5 groups onto B but only obtained a complex mixture of products. Synthesis of such a derivative, **135**, was achieved by Erker *et al.* incorporating Mes and C_6F_5 groups on P and B, respectively (Scheme 38).[85] NMR spectroscopy confirms the FLP nature of **135** with a tricoordinate B centre (^{11}B signal at 63.2 ppm) and lack of P→B interaction (^{31}P signal at -33.7 ppm). This is further supported by a large $\Delta\delta^{19}F_{m\text{-}p}$ (15.3 ppm).[27]

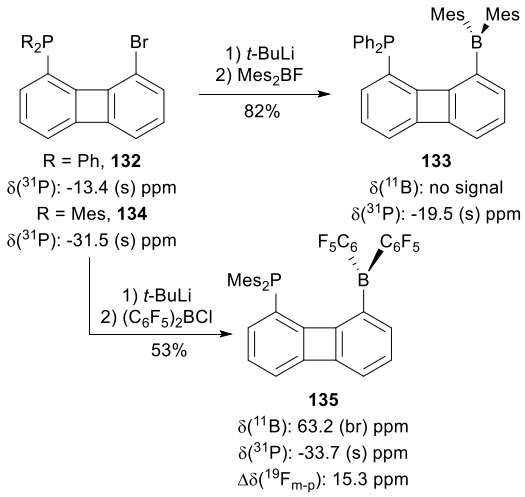

Scheme 38 Synthesis of the biphenylene-bridged P-B derivatives **133** and **135**.

While **135** itself could not be characterised in the solid state, **136**, its 1:1 adduct with the *N*-heterocyclic carbene I*t*Bu, could be isolated and analysed by X-ray diffraction (Scheme 39). As expected, the ^{11}B (-20.9 ppm) NMR signal now indicates a tetracoordinate B centre. This is confirmed in the solid state, finding a pyramidalized B centre ($\sum_{\alpha}$B = 359.5(1)°, THC = 78%). However, solid state analysis also revealed an unexpected connectivity with the B centre attached to a remote olefinic atom (C_4) and the respective hydrogen now bonded to the original carbene centre (C_2). Derivative **135** was found to readily react with H_2, providing the corresponding phosphonium borate **137** in 58% yield (Scheme 39). X-ray diffraction analysis of **137** shows that activation of H_2 results in pyramidalization of the B centre ($\sum_{\alpha}$B = 337.9(1)°, THC = 67%) and a H–H separation of 2.11(5) Å. Despite the close proximity of the hydridic and protic moieties in **137**, and an almost identical electronic situation to the dimethylxanthene-bridged derivative **116**, activation of H_2 is not reversible in this case. Nonetheless, the ability of **135** to activate H_2 could be leveraged towards catalysis. Metal-free hydrogenation of a bulky imine and an enamine was achieved with **137**.[85]

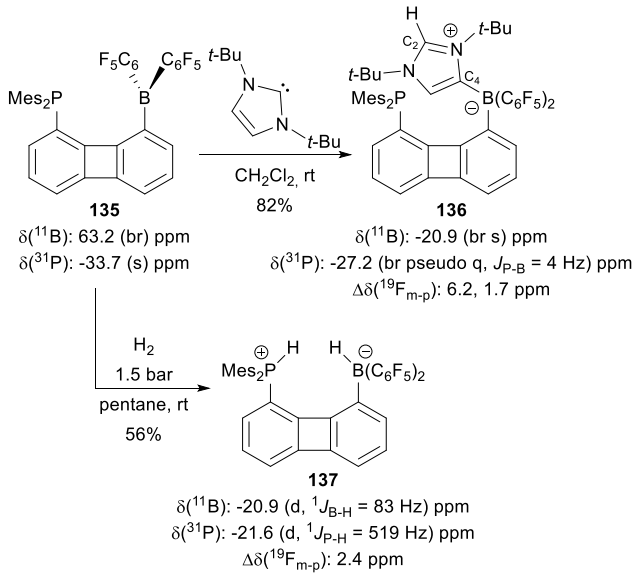

Scheme 39 Reaction of **135** with I*t*Bu and H_2.

In a similar fashion to the dimethylxanthene-bridged derivatives **113** and **114**, biphenylene **135** activates C(sp)–H bonds (Scheme 40).[85] Cyclopropylacetylene reacts with **135** in C_6D_6 at room temperature to provide the regioselective *trans* 1,2-addition product **138** in 72% yield, as confirmed spectroscopically and in the solid state (Scheme 40). The reaction of **135** with isopropenylacetylene at room temperature provides the C–H activation product **139a** and is reminiscent of the reactivity observed with **114**, showing apparent reversibility. Heating C_6D_6 solutions of **139a** induces formation of the *trans* 1,2-addition product **139**. *Trans* addition of the P-B compound **135** could be extended to phenylacetylene, 1-pentyne and 4-phenyl-1-butyne leading to **140**-**142**. The structures of **138**-**142** were unambiguously determined through multi-nuclear NMR spectroscopy and X-ray diffraction analyses.

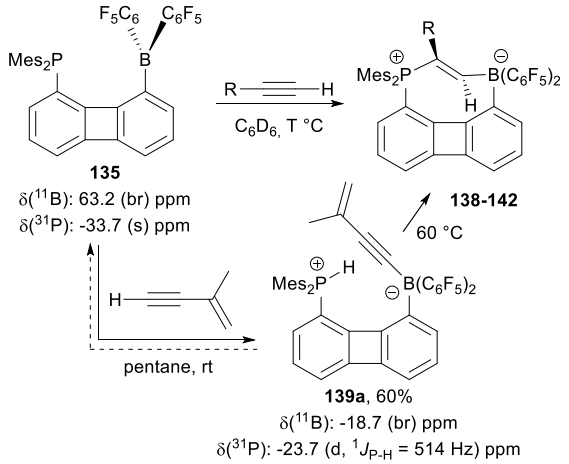

	R	Yield (%)	T °C	$\delta(^{11}B)$	$\delta(^{31}P)$
138	cyclopropyl	72	rt	-14.6	6.5
139	isopropenyl	65	60	-14.6	8.6
140	Ph	50	60	-15.2	11.8
141	*n*-C_3H_7	45	60	-14.9	5.3
142	$Ph(CH_2)_2$	13	60	-14.7	6.6

Scheme 40 *Trans* 1,2-addition of alkynes to **135**.

The biphenylene-bridged FLP **135** reacts with triplet dioxygen ($^3O_2$) to selectively furnish the dioxygenated product **143** (Scheme 41).[85] The structure of **143** is very reminiscent of the product we obtained in 2010 by reacting an *o*-phenylene P–B system with singlet dioxygen.[91] One oxygen sits on phosphorus and is actually engaged in a P–O–B bridge. The other one has inserted into one of the B–C_6F_5 bonds. Oxidation of the phosphine moiety is apparent from the ^{31}P NMR chemical shift (39.6 ppm) while the ^{11}B NMR signal at 8.2 ppm indicates a tetracoordinate B centre. The oxygenation product **143** was characterized in the solid state, finding P=O and O–B bond lengths of 1.527(1) and 1.569(2) Å, respectively, while the geometry about B is pyramidalized ($\Sigma_\alpha B$ = 341.1(1)°, THC = 70%). A radical pathway inspired from the reaction of trialkyl boranes with $^3O_2$ was proposed to account for the formation of **143**.

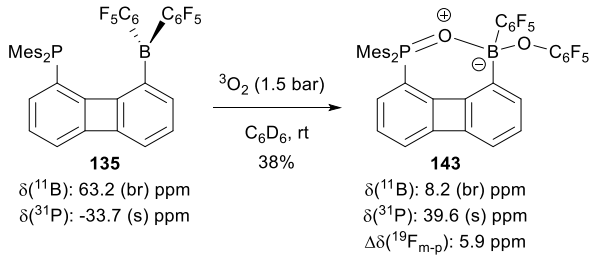

Scheme 41 Reaction of **135** with triplet dioxygen.

Finally, Erker *et al.* also demonstrated the ability of the biphenylene scaffold to form P-stabilised aryltriborane(7) compounds (Scheme 42).[86] Lithiation of **134** followed by trapping with an excess of $Me_2S{\cdot}BH_3$ and treatment with TMSCl provided derivative **144** in 50% yield (Scheme 42). In solution, **144** shows three distinct ^{11}B NMR signals at -8.6, -24.1 and -36.7 ppm. The latter is attributed to the P→B_2 unit due to the coupling observed ($^1J_{P\text{-}B}$ = 91 Hz), this coupling is also evident on examination of ^{31}P NMR spectra finding a broad signal at 7.8 ppm. The structure is hindered from rotation as evidenced by ^1H NMR at room temperature showing six distinct Me and four aromatic C-H signals

over both of the Mes groups. The structure of **144** was confirmed by X-ray diffraction analysis finding two independent molecules in the unit cell. They both display short P→B_2 interactions (1.943(6) and 1.963(4) Å, *r* = 1.02 and 1.03) and all B centres are significantly pyramidalized. Further derivatisation and reactivity of **144** was demonstrated by reacting it with two equivalents of $HB(C_6F_5)_2$ to provide the doubly C_6F_5-substituted product **145**. The structure of **145** was unambiguously confirmed by multi-nuclear NMR spectroscopy and X-ray diffraction.

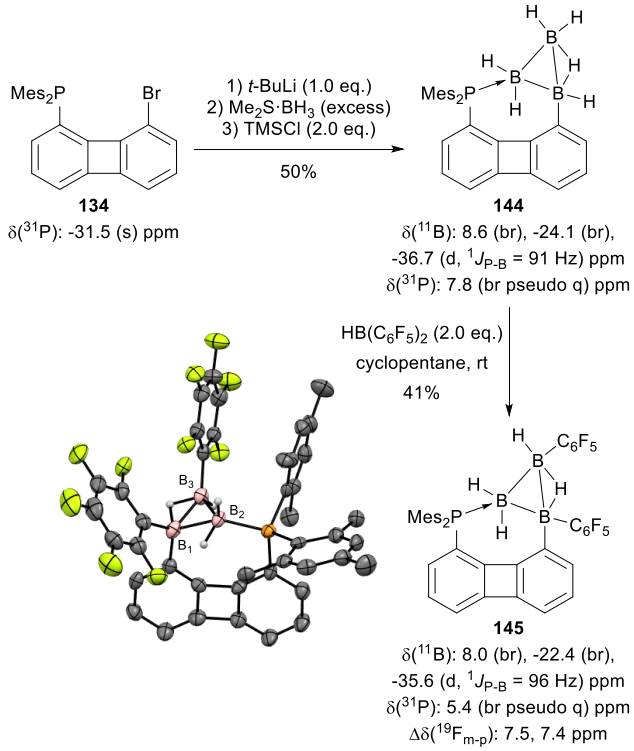

Scheme 42 Synthesis and reactivity of the P-stabilised aryltriborane(7) derivatives **144** and **145**; X-ray structure of **145** with carbon in grey, boron in pink, fluorine in green, phosphorus in orange, hydrogen in white, and the H atoms of the biphenylene backbone and Mes groups omitted for clarity.

8. Conclusions

As shown in this review, the combination of group 15 and group 13 elements on rigid carbon-based scaffolds give rise to original species presenting interesting structures and reactivity. To date, N-B and P-B derivatives are the most common among all possible E^{13}/E^{15} combinations, while the (ace)naphthalene and (thio)xanthene moieties have been the preferred scaffolds.

The unique geometric constraints imposed by (ace)naphthyl frameworks to the *peri*-substituents confer interesting structural and electronic properties to mixed E^{13}/E^{15} derivatives. The synthesis, structure and reactivity of these derivatives have been thoroughly investigated by several research groups, with theoretical calculations playing a vital role in deciphering and understanding the bonding/non-bonding interaction between the *peri*-substituents. Modulation of the steric and electronic nature of the donor and acceptor moieties at the *peri* positions enables to control and tune the D→A interaction. Additional control is provided by the choice of scaffold, where the naphthalene framework is shown to enforce E^{15}→E^{13} interactions while the acenaphthalene scaffold can be used to disrupt this interaction by increasing the *peri* distance. The resulting FLPs may be used to activate small molecules as shown with H_2O.

The other way around, the design of naphthalene compounds with strong D→A has been leveraged to prepare and study highly reactive species. A number of P-stabilised borenium cations have been reported and shown to display rich reactivity, especially regarding the activation of strong □-bonds (H_2, N–H). Using the same approach of geometrically enforced P-stabilisation, persistent boryl radicals with very high spin densities at boron have been prepared. Original radical reactivities have been substantiated, including Gomberg-type dimerization, halogen abstraction and hetero-coupling.

With rigid expanded spacers, E^{15}→E^{13} interactions are prevented geometrically. This results in enhanced and versatile ambiphilic behavior, as substantiated by the coordination properties of P-B thioxanthenes and FLP reactivity of P-B biphenylenes and xanthenes. Most noticeable is the impact of the rigid and preorganised structure of these systems on the reversibility of small molecule fixation/activation.

Given the progress achieved during the past two decades, it is likely that mixed E^{13}/E^{15} derivatives featuring rigid backbones will continue to attract much interest in the future. New synthetic methodologies are worth developing to enable straightforward and efficient introduction of the D and A groups. C–H activation approaches taking advantage of the D site as directing group are certainly worthwhile to explore. The nature of the D and A sites can also be varied further to include low-valent as well as high-valent moieties in particular, besides the common amine, phosphine and borane motifs mainly studied so far. Mixed E^{13}/E^{15} compounds hold great promise for small molecule activation and as ligands for transition metals. They may also open interesting avenues in other fields, such as chemical sensing, opto-electronic materials… The combination of E^{13} and E^{15} elements, and fine modulation of their interaction, are indeed very attractive to impart and control chemical and photophysical properties.

Acknowledgments

Support from the Centre National de la Recherche Scientifique, the Université de Toulouse and the Agence Nationale de la Recherche is gratefully acknowledged.

Notes and references

‡ For a review dealing with naphthalene derivatives *peri*-substituted with group 13 elements, see: J. D. Hoefelmeyer, M. Schulte, M. Tschinkl and F. P. Gabbaï, *Coord. Chem. Rev.*, 2002, **235**, 93–103. For reviews dealing with naphthalenes and related derivatives *peri*-substituted with group 15 and 16 elements, see: P. Kilian, F. R. Knight and J. D. Woollins, *Coord. Chem. Rev.*, 2011, **255**, 1387–1413 and P. Kilian, F. R. Knight and J. D. Woollins, *Chem. Eur. J.*, 2011, **17**, 2302–2328. For an early review dealing with *peri* interactions in naphthalene derivatives, see: V. Balasubramaniyan, *Chem. Rev.*, 1966, **66**, 567–641.

References

1 C. P. Brock and J. D. Dunitz, *Acta Crystallogr., Sect. B: Struct. Sci.*, 1982, **38**, 2218–2228.

2 A. C. Hazell, R. G. Hazell, L. Nørskov-Lauritsen, C. E. Briant and D. W. Jones, *Acta Crystallogr., Sect. C: Cryst. Struct. Commun.*, 1986, **42**, 690–693.

3 J. K. Fawcett and J. Trotter, *Acta Crystallogr.*, 1966, **20**, 87–93.

4 C. R. Groom, I. J. Bruno, M. P. Lightfoot and S. C. Ward, *Acta Crystallogr. Sect. B: Struct. Sci.*, 2016, **72**, 171–179.

5 J. A. Gillean III, D. W. Phelps and A. W. Cordes, *Acta Crystallogr. Sect. B*, 1973, **29**, 2296–2298.

6 O. Dideberg, L. Dupont and J. M. André, *Acta Crystallogr. Sect. B*, 1972, **28**, 1002–1007.

7 Z.-T. Jiang, B.-Q. Wang and Z.-J. Shi, *Chin. J. Chem.*, 2018, **36**, 950–954.

8 W. K. Chow, O. Y. Yuen, P. Y. Choy, C. M. So, C. P. Lau, W. T. Wong and F. Y. Kwong, *RSC Adv.*, 2013, **3**, 12518.

9 D. Pla, O. Sadek, S. Cadet, B. Mestre-Voegtlé and E. Gras, *Dalton Trans.*, 2015, **44**, 18340–18346.

10 S. Kawamorita, T. Miyazaki, H. Ohmiya, T. Iwai and M. Sawamura, *J. Am. Chem. Soc.*, 2011, **133**, 19310–19313.

11 Y. Kuninobu, T. Iwanaga, T. Omura and K. Takai, *Angew. Chem. Int. Ed.*, 2013, **52**, 4431–4434.

12 E. C. Keske, B. D. Moore, O. V. Zenkina, R. Wang, G. Schatte and C. M. Crudden, *Chem. Commun.*, 2014, **50**, 9883–9886.

13 J. A. Fernández-Salas, S. Manzini, L. Piola, A. M. Z. Slawin and S. P. Nolan, *Chem. Commun.*, 2014, **50**, 6782–6784.

14 S. Okada, T. Namikoshi, S. Watanabe and M. Murata, *ChemCatChem*, 2015, **7**, 1531–1534.

15 S. De Sarkar, N. Y. P. Kumar and L. Ackermann, *Chem. Eur. J.*, 2017, **23**, 84–87.

16 T. Ikawa, A. Takagi, Y. Kurita, K. Saito, K. Azechi, M. Egi, K. Kakiguchi, Y. Kita and S. Akai, *Angew. Chem. Int. Ed.*, 2010, **49**, 5563–5566.

17 A. Takagi, T. Ikawa, Y. Kurita, K. Saito, K. Azechi, M. Egi, Y. Itoh, H. Tokiwa, Y. Kita and S. Akai, *Tetrahedron*, 2013, **69**, 4338–4352.

18 H. Höpfl, *J. Organomet. Chem.*, 1999, **581**, 129–149.

19 E. Hupf, E. Lork, S. Mebs and J. Beckmann, *Organometallics*, 2015, **34**, 3873–3887.

20 A. J. Kirby and J. M. Percy, *Tetrahedron*, 1988, **44**, 6903–6910.

21 Š. Vyskočil, L. Meca, I. Tišlerová, I. Císařová, M. Polášek, S. R. Harutyunyan, Y. N. Belokon, R. M. J. Stead, L. Farrugia, S. C. Lockhart, W. L. Mitchell and P. Kočovský, *Chem. Eur. J.*, 2002, **8**, 4633–4648.

22 T. Leermann, F. R. Leroux and F. Colobert, *Org. Lett.*, 2011, **13**, 4479–4481.

23 R. L. Giles, J. A. K. Howard, L. G. F. Patrick, M. R. Probert, G. E. Smith and A. Whiting, *J. Organomet. Chem.*, 2003, **680**, 257–262.

24 B. Cordero, V. Gómez, A. E. Platero-Prats, M. Revés, J. Echeverría, E. Cremades, F. Barragán and S. Alvarez, *Dalton Trans.*, 2008, 2832.

25 S. Furan, E. Hupf, E. Lork, S. Mebs and J. Beckmann, *Eur. J. Inorg. Chem.*, 2017, **2017**, 3302–3311.

26 D. Winkelhaus, B. Neumann and N. W. Mitzel, *Z. Naturforsch., B: Chem. Sci.*, 2012, **67**, 589–593.

27 W. E. Piers, in *Adv. Organomet. Chem.*, 2004, vol. 52, pp. 1–76.

28 D. Winkelhaus, B. Neumann, H. G. Stammler, R. J. F. Berger, Y. V. Vishnevskiy and N. W. Mitzel, *Chem. Eur. J.*, 2012, **18**, 9312–9320.

29 M. Yamashita, K. Kamura, Y. Yamamoto and K. Akiba, *Chem. Eur. J.*, 2002, **8**, 2976.

30 C. Böker, M. Noltemeyer, H. Gornitzka, B. O. Kneisel, M. Teichert, R. Herbst-lrmer and A. Melier, *Main Group Met. Chem.*, 1998, **21**, 565–579.

31 G. S. Hair, S. L. Battle, A. Decken, A. H. Cowley and R. A. Jones, *Inorg. Chem.*, 2000, **39**, 27–31.

32 H. Schumann, S. Dechert, M. Hummert, K. C. H. Lange, S. Schutte, B. C. Wassermann, K. Köhler and J. Eichhorn, *Zeitschrift fur Anorg. und Allg. Chemie*, 2004, **630**, 1196–1204.

33 H. Schumann, B. C. Wassermann, S. Schutte, B. Heymer, S. Nickel, T. D. Seuß, S. Wernik, J. Demtschuk, F. Girgsdies and R. Weimann, *Z. Anorg. Allg. Chem.*, 2000, **626**, 2081–2095.

34 S. U. Ahmad and J. Beckmann, *Main Group Met. Chem.*, 2012, **35**, 29–33.

35 S. Bontemps, M. Devillard, S. Mallet-Ladeira, G. Bouhadir, K. Miqueu and D. Bourissou, *Inorg. Chem.*, 2013, **52**, 4714–4720.

36 J. Beckmann, E. Hupf, E. Lork and S. Mebs, *Inorg. Chem.*, 2013, **52**, 11881–11888.

37 Y. F. Li, Y. Kang, S. B. Ko, Y. Rao, F. Sauriol and S. Wang, *Organometallics*, 2013, **32**, 3063–3068.

38 S. Furan, E. Hupf, E. Lork and J. Beckmann, *Z. Anorg. Allg. Chem.*, 2021, zaac.202000480.

39 E. Hupf, E. Lork, S. Mebs, L. Chęcińska and J. Beckmann, *Organometallics*, 2014, **33**, 7247–7259.

40 A. Tsurusaki, T. Sasamori, A. Wakamiya, S. Yamaguchi, K. Nagura, S. Irle and N. Tokitoh, *Angew. Chem. Int. Ed.*, 2011, **50**, 10940–10943.

41 A. Tsurusaki, T. Sasamori and N. Tokitoh, *Chem. Eur. J.*, 2014, **20**, 3752–3758.

42 M. Yamashita, K. Watanabe, Y. Yamamoto and K. Akiba, *Chem. Lett.*, 2001, **30**, 1104–1105.

43 M. Devillard, R. Brousses, K. Miqueu, G. Bouhadir and D. Bourissou, *Angew. Chem. Int. Ed.*, 2015, **54**, 5722–5726.

44 M. Devillard, S. Mallet-Ladeira, G. Bouhadir and D. Bourissou, *Chem. Commun.*, 2016, **52**, 8877–8880.

45 M. Devillard, G. Bouhadir, S. Mallet-Ladeira, K. Miqueu and D. Bourissou, *Organometallics*, 2016, **35**, 3788–3794.

46 M. A. Dureen, A. Lough, T. M. Gilbert and D. W. Stephan, *Chem. Commun.*, 2008, **913**, 4303.

47 A. J. Rosenthal, M. Devillard, K. Miqueu, G. Bouhadir and D. Bourissou, *Angew. Chem. Int. Ed.*, 2015, **54**, 9198–9202.

48 A. J. Rosenthal, S. Mallet-Ladeira, G. Bouhadir, E.-D. Sosa-Carrizo, K. Miqueu and D. Bourissou, *Organometallics*, 2018, **37**, 755–760.

49 F. Dahcheh, D. Martin, D. W. Stephan and G. Bertrand, *Angew. Chem. Int. Ed.*, 2014, **53**, 13159–13163.

50 T. Matsumoto and F. P. Gabbaï, *Organometallics*, 2009, **28**, 4252–4253.

51 S.-H. Ueng, A. Solovyev, X. Yuan, S. J. Geib, L. Fensterbank, E. Lacôte, M. Malacria, M. Newcomb, J. C. Walton and D. P. Curran, *J. Am. Chem. Soc.*, 2009, **131**, 11256–11262.

52 J. C. Walton, M. M. Brahmi, L. Fensterbank, E. Lacôte, M. Malacria, Q. Chu, S.-H. Ueng, A. Solovyev and D. P. Curran, *J. Am. Chem. Soc.*, 2010, **132**, 2350–2358.

53 P. Bissinger, H. Braunschweig, A. Damme, I. Krummenacher, A. K. Phukan, K. Radacki and S. Sugawara, *Angew. Chem. Int. Ed.*, 2014, **53**, 7360–7363.

54 T. Kushida and S. Yamaguchi, *Organometallics*, 2013, **32**, 6654–6657.

55 R. G. Griffin and H. VAN Willigen, *J. Chem. Phys.*, 1972, **57**, 86–90.

56 L. Ji, R. M. Edkins, A. Lorbach, I. Krummenacher, C. Brückner, A. Eichhorn, H. Braunschweig, B. Engels, P. J. Low and T. B. Marder, *J. Am. Chem. Soc.*, 2015, **137**, 6750–6753.

57 J. E. Leffler, G. B. Watts, T. Tanigaki, E. Dolan and D. S. Miller, *J. Am. Chem. Soc.*, 1970, **92**, 6825–6830.

58 M. M. Olmstead and P. P. Power, *J. Am. Chem. Soc.*, 1986, **108**, 4235–4236.

59 M. Gomberg, *J. Am. Chem. Soc.*, 1900, **22**, 757–771.

60 M. Gomberg, *Chem. Rev.*, 1924, **1**, 91–141.

61 A. J. Rosenthal, S. Mallet-Ladeira, G. Bouhadir and D. Bourissou, *Synthesis*, 2018, **50**, 3671–3678.

62 M. Soleilhavoup and G. Bertrand, *Angew. Chem. Int. Ed.*, 2017, **56**, 10282–10292.

63 M. Soleilhavoup and G. Bertrand, *Chem*, 2020, **6**, 1275–1282.

64 A. D. Ledet and T. W. Hudnall, *Dalton Trans.*, 2016, **45**, 9820–9826.

65 M. Arrowsmith, D. Auerhammer, R. Bertermann, H. Braunschweig, G. Bringmann, M. A. Celik, R. D. Dewhurst, M. Finze, M. Grüne, M. Hailmann, T. Hertle and I. Krummenacher, *Angew. Chem. Int. Ed.*, 2016, **55**, 14464–14468.

66 M. Arrowsmith, J. I. Schweizer, M. Heinz, M. Härterich, I. Krummenacher, M. C. Holthausen and H. Braunschweig, *Chem. Sci.*, 2019, **10**, 5095–5103.

67 D. Lu, Y. He and C. Wu, *Phys. Chem. Chem. Phys.*, 2019, **21**, 23533–23540.

68 C. R. Wade, M. R. Saber and F. P. Gabbaï, *Heteroatom Chem.*, 2011, **22**, 500–505.

69 D. J. H. Emslie, J. M. Blackwell, J. F. Britten and L. E. Harrington, *Organometallics*, 2006, **25**, 2412–2414.

70 D. J. H. Emslie, B. E. Cowie and K. B. Kolpin, *Dalton Trans.*, 2012, **41**, 1101–1117.

71 S. R. Oakley, K. D. Parker, D. J. H. Emslie, I. Vargas-Baca, C. M. Robertson, L. E. Harrington and J. F. Britten, *Organometallics*, 2006, **25**, 5835–5838.

72 D. J. H. Emslie, L. E. Harrington, H. A. Jenkins, C. M. Robertson and J. F. Britten, *Organometallics*, 2008, **27**, 5317–5325.

73 D. J. H. Emslie, B. E. Cowie, S. R. Oakley, N. L. Huk, H. A. Jenkins, L. E. Harrington and J. F. Britten, *Dalton Trans.*, 2012, **41**, 3523–3535.

74 B. E. Cowie, D. J. H. Emslie, H. A. Jenkins and J. F. Britten, *Inorg. Chem.*, 2010, **49**, 4060–4072.

75 B. E. Cowie and D. J. H. Emslie, *Organometallics*, 2015, **34**, 2737–2746.

76 Z. Mo, E. L. Kolychev, A. Rit, J. Campos, H. Niu and S. Aldridge, *J. Am. Chem. Soc.*, 2015, **137**, 12227–12230.

77 Z. Mo, A. Rit, J. Campos, E. L. Kolychev and S. Aldridge, *J. Am. Chem. Soc.*, 2016, **138**, 3306–3309.

78 G. C. Welch, R. R. S. Juan, J. D. Masuda and D. W. Stephan, *Science*, 2006, **314**, 1124–1126.

79 B. L. Rinne, A. P. Lathem and Z. M. Heiden, *Dalton Trans.*, 2017, **46**, 9382–9393.

80 P. Vasko, I. A. Zulkifly, M. Á. Fuentes, Z. Mo, J. Hicks, P. C. J. Kamer and S. Aldridge, *Chem. Eur. J.*, 2018, **24**, 10531–10540.

81 M. Fleige, J. Möbus, T. vom Stein, F. Glorius and D. W. Stephan, *Chem. Commun.*, 2016, **52**, 10830–10833.

82 D. J. Parks, R. E. von H. Spence and W. E. Piers, *Angew. Chem. Int. Ed. English*, 1995, **34**, 809–811.

83 P. Vasko, M. Á. Fuentes, J. Hicks and S. Aldridge, *Dalton Trans.*, 2019, **48**, 2896–2899.

84 F. Kutter, E. Lork and J. Beckmann, *Z. Anorg. Allg. Chem.*, 2018, **644**, 1234–1237.

85 J. Li, C. G. Daniliuc, G. Kehr and G. Erker, *Chem. Commun.*, 2018, **54**, 6344–6347.

86 J. Li, C. G. Daniliuc, G. Kehr and G. Erker, *Chem. Commun.*, 2018, **54**, 12606–12609.

87 L. L. Zeonjuk, N. Vankova, A. Mavrandonakis, T. Heine, G.-V. Röschenthaler and J. Eicher, *Chem. Eur. J.*, 2013, **19**, 17413–17424.

88 G. Skara, B. Pinter, J. Top, P. Geerlings, F. De Proft and F. De Vleeschouwer, *Chem. Eur. J.*, 2015, **21**, 5510–5519.

89 G. Bistoni, A. A. Auer and F. Neese, *Chem. Eur. J.*, 2017, **23**, 865–873.

90 Y. Shao, J. Zhang, Y. Li, Y. Liu and Z. Ke, *Org. Lett.*, 2018, **20**, 1102–1105.

91 S. Porcel, G. Bouhadir, N. Saffon, L. Maron and D. Bourissou, *Angew. Chem. Int. Ed.*, 2010, **49**, 6186–6189.

Entry for the Table of Contents